https://doi.org/10.15407/ufm.27.01.084

A.Z. ISSAGULOV*, V.Yu. KULIKOV, S.V. KVON***,
S.K. ARINOVA****, and A.A. TUGANBAYEVA*******

Abylkas Saginov Karaganda Technical University,
56 Nursultan Nazarbayev Ave., 100003 Karaganda, Kazakhstan

* a.issagulov@ktu.edu.kz, ** v.kulikov@ktu.edu.kz, *** s.kvon@ktu.edu.kz,
**** s.arinova@ktu.edu.kz, ***** dicosia0789@gmail.com

CURRENT TRENDS IN THE PRODUCTION OF FERROUS AND NON-FERROUS ALLOYS' CASTINGS USING EXTERNAL AND INTERNAL INFLUENCES

This review synthesises the state of the art in refining and homogenising metal-alloy structures through internal chemical modifications and external physical fields. The mechanisms, by which nanoparticles, rare-earth elements, and inoculants promote heterogeneous nucleation and control crystallisation dynamics, are analysed. The impact of mechanical oscillations, ultrasonic treatment, and electromagnetic fields on grain morphology, phase uniformity, and inclusion behaviour is evaluated. Particular attention is focused on the synergistic action of these methods to produce reinforced or composite-like microstructures with enhanced mechanical and functional performance. The review critically assesses existing knowledge and proposes a conceptual framework for further investigation of melt-processing strategies aimed at creating materials with tailored properties for advanced applications.

Keywords: internal modification, external fields, crystallisation mechanisms, heterogeneous nucleation, synergistic processing, alloy microstructure.

Citation: A.Z. Issagulov, V.Yu. Kulikov, S.V. Kvon, S.K. Arinova, and A.A. Tuganbayeva, Current Trends in the Production of Ferrous and Non-Ferrous Alloys' Castings Using External and Internal Influences, *Progress in Physics of Metals*, **27**, No. 1: 84–129 (2026)

1. Introduction

The operating conditions of equipment in the mining and metallurgical sector are highly demanding, characterised by elevated temperatures, increased wear, exposure to gas corrosion, heavy loads and extended service life. Accordingly, the materials employed in this sector must meet stringent requirements with respect to both fundamental properties (strength, hardness, impact toughness) and specific properties (such as wear resistance and heat resistance). Evidently, achieving such properties necessitates the use of either specially designed alloys or complex alloyed steels for manufacturing purposes [1].

However, the potential for further improvement of material properties through the use of additional alloying elements or enhanced heat treatment has largely been exhausted. Moreover, the development and industrial implementation of such new technologies require considerable material and time investments.

One of the contemporary approaches to enhancing the properties of complex alloyed steels involves the application of various methods of influence, including, for example, nanomodification, mechanical vibration, magnetic field treatment, ultrasound, and other external effects applied to the melt.

Notably, nanomodification has emerged as a key trend in improving the properties of alloy steels [1–11]. Steels treated in this way are regarded as reinforced or next-generation composite materials [4, 7, 10]. Numerous studies have demonstrated that introducing nanoparticles of refractory compounds into the melt of alloyed steel results in grain refinement and improvements in hardness and strength. In some cases, nanomodification also enhances specific properties, such as wear resistance and heat resistance.

Earlier studies [12–14] by the authors of the present programme reported the influence of inoculants and nanomodifiers of various types on the structural and strength characteristics of alloy steels. These studies revealed a clear positive trend in the effects of both inoculants and nanomodifiers on steel properties. The results previously obtained by the authors are intended to underpin the development of technology for producing complex alloyed steels with a homogeneous, defect-free structure, achieved through the synergistic application of internal and external influences on the melt.

Another widely recognised approach to improving the properties of alloy steels is the application of out-of-furnace treatments to the melt, including vibration, ultrasonic processing and magnetic field effects [15–22].

In Ref. [16], the dependence of alloy properties on the application of magnetic field, ultrasonic, and vibrational effects during crystallisation was examined and analysed. The study noted that, despite discrepancies in the reported quantitative effects of external factors on the mechanical properties of alloys, their qualitative influence is evident in the enhancement of strength characteristics under the action of magnetic field, ultrasonic, and vibrational treatment.

Reference [17] presents research findings on the influence of a magnetic field on the strength and conditional yield strength of 35CrM steel. Engine components, manufactured both by conventional methods and with additional exposure to a magnetic field, were investigated as samples. The study reported an increase in ultimate strength by 12–15% and a rise in dislocation density. Improved structural homogeneity, achieved through magnetic treatment, contributed to a reduction in microdefects and, consequently, an improvement in the overall mechanical properties of the alloy.

Further evidence of alloy property enhancement due to magnetic field treatment is provided in Refs. [18–20]. These studies, which investigated different materials (including aluminium alloys and various steel grades), demonstrated that magnetic fields promote an increased nucleation rate during the initial stage of primary crystallisation, a reduction in grain size, and lower dislocation density. The extent of the magnetic fields' effect was shown to depend on its specific parameters. A 'memory effect' of magnetic treatment, persisting for approximately 5–15 minutes, was also reported.

In Ref. [21], the positive effect of external treatment on the microstructure and properties of copper alloy composites was demonstrated, with increases in strength, yield strength, and elongation observed.

It is noteworthy that the previous literature analysis unequivocally confirms the feasibility of combining nanomodification with the simultaneous application of external mechanical or magnetic effects in steel processing. However, in all cited studies, nanomodification was conducted directly in the furnace, while magnetic fields or mechanical vibration were applied as subsequent operations in steel processing.

2. Modern Alloy Production Using Modifiers (Internal Treatment)

The microstructure and mechanical properties (impact toughness, tensile strength, and hardness) of Al–7Si and Al–7Si–2.5Cu casting alloys have been investigated following various melt treatments, including milling and grain modification [22]. The results demonstrate that Al–7Si–2.5Cu alloys subjected to milling and grain modification exhibit a microstructure characterised by uniformly distributed α-Al grains, an interdendritic eutectic network of fine silicon particles, and small $CuAl_2$ particles within the interdendritic regions. These alloys showed superior mechanical properties in the as-cast condition compared to alloys treated solely by refining or modification. The improvement in the mechanical properties of the Al–7Si–2.5Cu alloys is attributed to the breakdown of coarse aluminium grains and to the uniform distribution of eutectic silicon and fine $CuAl_2$ particles within the interdendritic areas, resulting from the combined refining and modification processes. The study also sought to evaluate the effect of microstructural changes in Al–7Si and Al–7Si–2.5Cu foundry alloys on their mechanical properties (impact toughness, tensile strength, and hardness) through grain refinement, modification, and their combined application.

The aluminium alloy ZL114A is a typical Al–Si casting alloy renowned for its excellent casting performance and high strength, making it suitable for producing various large castings and components. However, the refinement of coarse α-Al grains under sand mould casting conditions remains challenging and has been rarely addressed in detail. In Ref. [23], a combined strategy was investigated, involving the addition of a novel grain-refinement agent, Al–TCB (comprising complex C–TiB_2 and B–TiC particles) together with an Al–Sr modifier to ZL114A alloy cast in sand moulds. It was shown that the combined use of Al–TCB and the Sr modifier provides more favourable modification conditions than the use of Sr alone, indicating a pronounced synergistic effect. With the addition of the Sr modifier alone, the average α-Al grain size and the average eutectic Si length in ZL114A were reduced to 320 μm and 10.05 μm, respectively, compared to 404.2 μm and 22 μm. When the Sr modifier and Al–TCB grain refiner were applied simultaneously, the average α-Al grain size and eutectic Si length were further reduced to 183.4 μm and 3.34 μm, corresponding to reductions of 54.6% and 84.8%, respectively. After T6 heat treatment, the ultimate tensile strength (UTS) of the ZL114A alloy modified with Sr and Al–TCB increased to 290 ± 5.4 MPa, approximately 71.6% higher than that of the alloy treated with Sr alone. In addition, the elongation to fracture (EL) increased significantly from $1.4 \pm 0.34\%$ to $8.4 \pm 0.02\%$, representing a 500% improvement. Microstructural characterisation and electron probe microanalysis confirmed that there was no discernible segregation of silicon at the interface between the nucleated C–TiB_2 particles and the aluminium matrix, indicating that silicon atoms neither participate in nor interfere with the nucleation process. Consequently, the poisoning effect of silicon can be avoided under these conditions, leading to superior mechanical properties. These findings are expected to provide valuable guidance for improving the microstructure and optimising the mechanical properties of Al–Si alloys in industrial applications.

Recycling aluminium waste contributes to conserving aluminium resources, saving energy, and protecting the environment. Iron is the principal detrimental impurity in aluminium waste, and its removal is essential. Typically, an iron-removing element (M) is added to the Al–Si–Fe system to enhance iron removal efficiency through physical separation. However, excess M in the aluminium waste subsequently becomes a harmful impurity itself and must also be eliminated. The critical iron content ($Fe_{critical}$) and critical M content ($M_{critical}$) in Al–Si-based scrap are key factors in calculating the theoretical maximum recovery rates of iron (R_{Fe}) and M (R_M) achievable by most physical separation techniques. Nevertheless, determining these critical contents in multicomponent Al–Si-based alloys is challenging.

The study reported in Ref. [24] proposes the use of the electromagnetic directed crystallisation (EDC) technique for separating Al–Si–(Fe, Ni) melts. This approach simultaneously achieves four objectives: determining $Fe_{critical}$ and $Ni_{critical}$, reducing the Fe and Ni contents to their critical levels, producing eutectic Al–Si–(Fe, Ni) alloys, and transforming harmful iron needle-like phases into benign ones. Furthermore, the $Fe_{critical}$ value was reduced from 0.5% to 0.378±0.04% in the Al–Si–Fe alloy and to 0.30±0.04% in the Al–Si–Fe–Ni alloy, confirming the theoretical positive effect of Ni addition on Fe removal. The critical Ni content in the Al–Si–Fe–Ni alloy was found to be 4.4±0.12%, slightly lower than that in the Al–Si–Ni alloy (4.6±0.21%). In other words, Ni added for Fe removal was effectively eliminated along with Fe by the EDC process, without accumulating in the aluminium–silicon waste.

In Ref. [25], the effects of microalloying with Er, Zr, V, and Ti, combined with deep melt purification in a multipole field, on the microstructure and mechanical properties of Al–12Si–4.5Cu–2Ni alloy were investigated. Phase diagram calculations and DSC (differential scanning calorimetry) curves revealed that the second-phase constituents of the microalloyed Al–12Si–4.5Cu–2Ni alloy predominantly comprised AlCuNi, $(Al, Si)_3(Zr, Ti, V)$–$D0_{22}/D0_{23}$, Al_2Cu, $Al_3(Zr, Er)$, and Al_2Si_2Sr phases. The solidus and liquidus temperatures were determined to be 518.1 °C and 597.4°C, respectively. The addition of erbium significantly refined the grains and facilitated the formation of $L1_2$–$Al_3(Zr, Er)$ precipitates coherently aligned with the α-Al matrix. The microalloying elements reduced the dislocation energy in the alloy, resulting in extensive dislocation networks within both the α-Al matrix and eutectic Si. Moreover, degassing with Ar combined with an ultrasonic field not only reduced the pore size and number of pores in the ingot but also improved the uniformity of the second-phase distribution. As a result of microalloying and multi-field degassing, the alloy exhibited yield strength, tensile strength, and elongation of 163.9 MPa, 300.2 MPa and 3.2%, respectively. The second-phase constituents of the microalloyed Al–12Si–4.5Cu–2Ni alloy were systematically characterised, providing a basis for the future design of heat-resistant aluminium alloys and for defining subsequent heat-treatment parameters.

The microstructure, static mechanical properties (tensile strength and fracture toughness), and dynamic mechanical properties (impact toughness) of Al–7Si–0.3Mg-based alloys with the addition of various grain refiners and modifiers have been investigated [26]. In particular, the effect of increasing phosphorus content (up to 40 ppm) on the efficacy of modifiers in Al–7Si–0.3Mg-based alloys with a high impurity level was studied. The findings can be summarised as follows: (i) the shape factor of eutectic Si increased with rising Eu content and decreasing P content; (ii) the base Al–7Si–0.3Mg alloy and the conventionally refined Al–5Ti–1B alloy modified with Sr exhibited the highest elongation (≈11%) in the T6 condition, compared with alloys refined with Ta and modified with Eu, while further increases in Eu and/or P reduced elongation; (iii) the shape factor was found to influence impact toughness, necessitating appropriate modification and heat treatment; (iv) impact toughness increased with increasing Eu content and decreasing P content; (v) Ta- and Eu-rich intermetallic phases were observed on the fracture surface; (vi) a fractured Eu-rich intermetallic phase (Al_2Si_2Eu) was identified on the fracture surface, indicating no significant improvement in mechanical properties due to the presence of brittle intermetallic phases; (vii) the impact toughness of the alloy with 200 ppm Eu was marginally higher than that of the alloy with 200 ppm Sr, while Eu modification did not lead to an increase in elongation despite the microstructural data reported here and in the literature. This study provides new insights into the effects of melt treatment, specifically, increased α-Al dispersity, modification of eutectic Si, and enhanced dispersity of eutectic grains, using Ta and Eu on the static and dynamic mechanical properties of Al–7Si–0.3Mg-based alloys.

The authors also conducted a literature review on this topic and explored the potential of using microsilica (a by-product of silicon production) as a modifier to develop new materials with tailored properties [27].

The microstructure and properties of recycled AA3104 alloy are significantly affected by impurities such as Fe and Si. To address this, Al–Sr–RE was proposed in Ref. [28] as a means of improving the microstructure and mechanical properties of AA3104 alloy with high Fe content. Scanning electron microscopy (SEM), differential scanning calorimetry, thermodynamic calculations, and synchrotron X-ray computed tomography (SXRCT) were employed to investigate the morphological characteristics and solidification path of Fe-rich phases. The results indicated that the addition of trace amounts of Sr or Ce to Al–5Ti–1B alloy did not markedly alter the grain structure, while the addition of Al–8Sr–8Ce alone did not significantly affect the α-Al matrix. However, Al–8Sr–8Ce transformed the two-dimensional morphology of the Fe-rich phases from hieroglyphic to skeletal and short-rod shapes, and the three-dimensional morphology from a lamellar branched structure to a rod-like branched structure. The average equivalent diameter of the Fe-rich phases decreased by 12.16% relative to the Al–Ti–B alloy, while the average sphericity increased by 5.00%. The addition of trace amounts of Sr or Ce based on Al–5Ti–1B, as well as Al–8Sr–8Ce, improved the mechanical properties of the alloy. Notably, the Al–Sr–Ce-modified alloy exhibited optimal mechanical properties, with tensile strength, yield strength, and elongation increasing by 7.77%, 10.87% and 24.06%, respectively. This study presents a novel modifier for altering the Fe-rich phases in recycled Al–Mn–Mg alloys with high iron content.

A hypereutectic aluminium–silicon alloy (AlSi18) was modified using a conventional modifier, namely, phosphorus (P), and by simultaneously introducing both the conventional modifier (P) and a nanomodifier, *i.e.*, nanodiamonds (ND), into the melt [29]. The effects of these modifications on the microstructure and mechanical properties of the alloy were investigated. The results demonstrated that the structure was refined and the mechanical properties were enhanced. The influence of the two modifiers on both the primary silicon crystals and the eutectic phases of the alloy is discussed.

Strontium and Al–Ti–B grain refiner were simultaneously added to an Al–7Si–0.35Mg cast alloy, and the interaction between Sr and Al–5Ti–1B was examined [30]. The combined additions of 100 ppm Sr and 500 ppm Ti resulted in both modification of the eutectic Si and refinement of the α-Al grains, while increasing the nucleation frequency of eutectic Al–Si grains compared with the alloy modified with Sr alone. Phase electron microscopy (PEM) analysis revealed the presence of Al_2Si_2Sr phases in association with either TiB_2 or AlP and TiB_2 bonding particles. This suggests that the pre-existing TiB_2 particles in the melt facilitated the formation of significant quantities of AlP (the most effective nucleation sites for Si), which, in turn, promoted the nucleation of eutectic Al–Si grains during solidification, despite the partial deactivation of AlP consumed in the earlier formation of Al_2Si_2Sr.

In Ref. [31], the performance of an Al–7%Si–0.35%Mg alloy (A356 alloy) was enhanced by modifying its microstructure. The ultimate tensile strength was increased through the addition of strontium (Sr), overheating, or melt heat treatment combined with Sr addition, whereas heat treatment of the melt alone had a negligible effect on UTS. Both Sr modification and Sr-modified melt heat treatment improved the elongation of A356 alloy castings, with greater elongation achieved at higher cooling rates. The effects of solution heat treatment on the tensile properties of A356.2 alloy castings can be summarised as follows: (i) the yield strength is significantly improved after eight hours of solution treatment due to the precipitation of Mg_2Si; (ii) extending the solution treatment up to 80 hours results in little further change in yield strength; and (iii) UTS is significantly enhanced during the initial eight hours and continues to increase up to 80 hours, attributed to Mg_2Si precipitation, silicon dissolution in the Al matrix, and spheroidization of Si. The ductility of A356.2 alloys was also improved markedly by solution treatment, rising from approximately 6% in the as-cast condition to around 10% after 80 hours of treatment.

The microstructural evolution, segregation behaviour, and fracture mechanism of an A390 hypereutectic alloy produced by Rheo-HPDC (high-pressure die casting) with Sr modification were investigated using morphological analysis and electron probe microanalysis (EPMA) [32]. The results showed that Rheo-HPDC with Sr modification simultaneously refined the primary silicon particles (PSPs) and modified the eutectic silicon. Strontium reduced the tendency of dendritic α-Al halos to form around PSPs by narrowing the constitutionally supercooled zone at the solid–liquid interface, promoting eutectic silicon formation on the primary silicon. Liquid segregation caused the PSPs to concentrate at the centre of the sample, while other alloying elements segregated towards the edges. Trace amounts of Sr enhanced elemental segregation by increasing the melt viscosity; however, as the Sr content increased, the melt viscosity gradually decreased.

Aluminium-based metal matrix composites reinforced with carbon nanotubes (CNTs) are regarded as highly promising materials for a range of industrial applications owing to the excellent reinforcing properties of CNTs. The addition of CNTs to aluminium and its alloys can significantly enhance their physical, mechanical, thermal, and electrical properties. To date, numerous aluminium alloys containing scandium have been studied. However, to the best of our knowledge, there is almost no comprehensive information in the open literature on Al–Sc alloys produced by melt spinning, nor on Al–2Sc alloys produced by melt spinning with CNT addition. In Ref. [33], Al–2Sc ribbons were successfully produced by melt spinning with CNT addition, and the effects of CNTs on the morphology, microhardness, and electrical properties were investigated. The resulting microstructures, as well as thermal, mechanical, and electrical characteristics, were analysed using x-ray diffraction, scanning electron microscopy, Vickers microhardness testing, and four-point resistivity measurements.

Cast Al–Si alloys are characterised by inherently low ductility due to coarse α-Al grains and large lamellar eutectic Si. Although boron-containing grain refiners and Sr modifiers can refine α-Al grains and eutectic Si, respectively, their simultaneous addition leads to an unacceptable reduction in the effectiveness of Sr because boron exerts a poisoning effect on Sr in Al–10Si–B–Sr alloys. In Ref. [34], it was demonstrated that both α-Al grain refinement and Si modification can be achieved by simply adding 500 ppm La to an Al–10Si–0.02B–0.015Sr alloy, significantly improving ductility and tensile strength. In the Al–10Si–0.02B–0.015Sr melt, Sr interacts with B to form a Sr–B intermetallic compound, consuming Sr and diminishing its modifying effect. CALPHAD-type calculations showed that the Sr concentration in the liquid before the eutectic reaction becomes a key parameter in evaluating the effectiveness of alloy modification. The addition of La promotes the formation of LaB_6, which stabilises the Sr-modifying effect by releasing Sr. First-principles calculations further indicated that both Sr and La promote the formation of twin boundaries in Si particles by lowering the twin boundary formation energy. LaB_6 forms a semi-coherent interface with α-Al, with the orientation relationship $[1\bar{1}0]LaB_6//[1\bar{1}0]Al$ and $[1\bar{1}1]LaB_6//[1\bar{1}1]Al$, demonstrating that LaB_6 acts as an effective α-Al nucleation centre and facilitates α-Al refinement in the Al–10Si–0.05La–0.02B–0.015Sr alloy. These results elucidate the micromechanism of refinement during solidification and offer an efficient and simple method for producing high-performance aluminium alloys.

The effect of a complex modifier, 3Be–Sb (Be:Sb ratio equal to 3), on the microstructure and mechanical properties of a hypereutectic Al–Si–Mg alloy was investigated in Ref. [35]. The addition of 0.2 wt.% 3Be–Sb transformed the primary α-Al phase from dendritic to equiaxed, significantly refined the eutectic Si phase, and reduced the size of primary Mg_2Si. Further increasing the 3Be–Sb content to 0.6 wt.% resulted in a complete morphological change of the Mg_2Si phase from square to spherical and maximised the refining effect on the primary α-Al phase.

Phosphorus is an effective modifier that significantly reduces the size of primary silicon (Si) crystals. However, beyond a certain content of P, the modifier tends to aggregate, reducing its refining efficiency. In Ref. [36], the evolution of the microstructure and mechanical properties of an Al–50Si alloy was studied by combining superheating and modification treatments. After modification, the average size of the primary Si phase increased with increasing superheating temperature, while the overall hardness decreased. Notably, when the modifier content reached 7 wt.%, the alloy exhibited its highest hardness, even though it was considered overmodified. Nanoindentation tests revealed that the nanohardness of the Al_2Cu intermetallic phase was 5.52 GPa, *i.e.*, three times higher than that of the Al matrix, explaining the increased hardness of the alloy after remodification. These findings indicate that, in addition to the size and distribution of the primary Si phase, compounds such as Al_2Cu play an important role in enhancing the mechanical properties of the alloy. The melting process of the alloy was observed *in situ* using a laser confocal high-temperature scanning microscope, and it was found that the melting temperature of α-Al decreased with increasing Cu content in the matrix. A strain energy calculation model was proposed and validated, showing that the strain energy increased progressively with increasing Cu content, which was identified as the primary factor behind the reduction in the matrix melting temperature. The existence of strain energy was further confirmed by the electron backscatter diffraction (EBSD) analysis.

In Ref. [37], the causes of instability in the chemical composition and mechanical properties of low-carbon alloy steels were analysed, and potential solutions were proposed. It was found that instability in chemical composition and the presence of elongated, sharp-edged non-metallic inclusions — containing excessive amounts of gas and other impurities —

shorten the service life of the finished metallurgical product and degrade its quality. As established and demonstrated, one effective approach to stabilising the chemical composition and enhancing the mechanical properties, as well as the overall quality of reinforcement steel, is to treat the steel melt with multifunctional modifiers.

The production of semi-solid slurry from aluminium alloy A356 using an inclined plate was investigated in [38]. As the A356 alloy melt flowed down an inclined plate cooled from below by a countercurrent of water, it partially solidified, leading to the continuous formation of columnar dendrites on the plate surface. Owing to forced convection, these dendrites fragmented into equiaxed grains, which were then washed away to form semi-solid slurry at the exit of the plate. The melt pouring temperature ensured the appropriate solidification conditions, while the plate inclination provided the required shear to produce semi-solid slurry of the desired quality. The resulting slurry was solidified in a metal mould to produce semi-solid castings with a refined microstructure. Heat treatment was subsequently applied to the castings to improve surface quality. The effects of melt pouring temperature and plate tilt angle on the solidification process and microstructure of the castings were described. Four melt pouring temperatures (620, 625, 630 and 635 °C) and four tilt angles (30°, 45°, 60°, and 75°) were investigated. The optimal conditions, yielding a fine-grained, globular microstructure, were identified as a pouring temperature of 625 °C and a plate tilt angle of 60°.

In Ref. [39], the combined effect of microstructural modification through the addition of Ti, B, Ni, and Cr alloying elements, together with heat treatment, homogenisation, and solution treatment (T6), on the mechanical and dynamic properties of an Al–Zn–Mg–Cu-based aluminium alloy was investigated. The cast alloys underwent homogenisation at 470 °C for 3 h, air-cooling, solution treatment at 470 °C for 3 h, quenching, and artificial ageing at 120 °C for 24 h. The modified Al–Zn–Mg–Cu alloy exhibited an improved microstructure compared to the unmodified alloy, particularly after T6 treatment, as confirmed by scanning electron microscopy. The T6 treatment enhanced the microstructure by dissolving intermetallic phases and dispersoids, followed by quenching and ageing, which promoted the precipitation of strengthening phases. The modified alloy showed an 11.4% increase in tensile strength and a 40% increase in elongation compared to the as-cast alloy.

The modifying effect of tellurium (Te) and the growth process of Mg_2Si were studied in Ref. [40]. The addition of 0.5 wt.% Te transformed dendritic primary Mg_2Si into a polygonal form, reducing its size from over 165 μm to 18 μm. However, increasing the Te content to 2 wt.% diminished the modifying effect, and the Mg_2Si reverted to a dendritic morphology. Three-dimensional morphology analysis showed that Te modified the primary Mg_2Si by transforming dendrites into polyhedra bounded by {111} and {100} planes. The modification mechanism of Te was attributed to heterogeneous nucleation and Te incorporation during the growth of primary Mg_2Si, which significantly contributed to the reduction in size and morphological change.

The aim of Ref. [41] was to investigate the combined effect of an Al–5Ti–1B master alloy and modified strain-induced melt activation (SIMA) process on the structural characteristics, mechanical properties, and dry friction behaviour of an Al–12Zn–3Mg–2.5Cu aluminium alloy. The optimum Ti content in the master alloy for effective grain refinement was determined to be 2 wt.%. The alloy was produced using a modified SIMA process, with reheating conditions optimised to obtain a fine-grained, globular microstructure at 575 °C for 20 minutes. All specimens underwent T6 heat treatment prior to tensile testing. The combination of the grain refiner and T6 treatment led to significant improvement in mechanical properties: after T6 treatment, the average tensile strength increased from 283 MPa to 587 MPa in specimens without SIMA processing, and from 252 MPa to 564 MPa in those subjected to SIMA processing. The wear resistance of the alloy under dry sliding conditions was also examined. The results showed that T6 treatment significantly improved wear resistance. However, the ultimate strength and dry sliding wear resistance of specimens with a globular microstructure were lower than those of titanium-hardened specimens produced without SIMA processing.

In Ref. [42], the effect of individual and combined additions of refining and modifying agents on the mechanical properties, microstructure, grain refinement and modification, and intermetallic compounds of melt-cast Al–7.5Si–4Cu alloy was comparatively investigated. The alloy was modified with Al–5Ti–B, rare earths (RE), and Al–10Sr, and cast into chromium sand moulds. The results showed that the combined addition of 0.8 wt.% Al–5Ti–B, 0.1 wt.% RE, and 0.1 wt.% Al–10Sr as refiners and grain modifiers significantly improved the mechanical properties and microstructure of the cast alloy compared to individual additions and baseline casting conditions. When 0.8 wt.% Al–5Ti–B was added individually, the alloy exhibited higher tensile strength, Brinell hardness, and finer equiaxed α-Al dendrites. The alloy modified with 0.1 wt.% rare earths showed the best ductility, as rare earth elements purified the melt and altered the morphology of intermetallic compounds. In contrast, the alloy modified with 0.1 wt.% Al–10Sr showed an improvement in yield strength, but other properties were unsatisfactory. While Al–10Sr effectively modified the eutectic silicon, it also increased the gas content in the melt, resulting in the formation of coarse columnar grains. The trends in grain refinement and modification, as reflected by the average area and aspect ratio, were consistent with the mechanical property and microstructure analyses.

In Ref. [43], an Al–9Zr–0.9Sr master alloy was used as a refiner and modifier for Al–7Si–0.5Mg alloy. A melt sputtering technique was applied to reduce the particle size and improve the morphology of the master alloy particles, thereby enhancing the refining and modifying effects of Al–9Zr–0.9Sr. The refining mechanism was discussed in detail. The melt treatment reduced the size of second-phase particles in the master alloy from micrometres to nanometres, improving their distribution within the matrix. Adding 3 wt.% inoculating tape reduced the grain size of the alloy from 358 ± 48 μm to 122 ± 16 μm, and the needle-like eutectic silicon was completely transformed into fibrous silicon. In the Al–7Si–0.5Mg alloy, Al_3Zr in the inoculant reacted with Si to form (Al, Zr, Si), which replaced Al_3Zr as the heterogeneous nucleation site for α-Al, enabling effective grain refinement.

In Ref. [44], the combined modification process of P and Sr in Al–30Si hypereutectic alloys was studied. The continuous addition of 2.0 wt.% Al–3P and 0.7 wt.% Al–10Sr during alloying and solidification significantly refined the primary Si from over 200.0 μm to 32.8 μm with uniform distribution, while modifying the eutectic Si into a fibrous morphology. The modification mechanism was also examined. The melt temperature influenced the interaction between P and Sr. At approximately 1000 °C, AlP became encapsulated by an Al_4Sr phase, which reacted with Sr at ≈1300 °C to form Sr_3P_2. At 770 °C, P and Sr existed in the forms of AlP and Al_4Sr, respectively, which was identified as the key to achieving excellent combined modification of the Si phase during continuous refining.

Metal–polymer systems using modifiers are also being explored. Polymer modification is a promising approach to enhancing the performance of injection-moulded direct joining (IMDJ). However, the mechanisms contributing to joint strength at the submicron scale remain unclear. In Ref. [45], the mechanism of improved joint performance between polyamide 6 (PA6) and A5052 aluminium alloy pre-treated by blasting, hot water treatment, and a flow modifier (OSGOL MF-11) was investigated. Increased mechanical interlocking of the polymer at the submicron level was confirmed, along with hydrogen bond formation at the interface of the joined materials. These findings elucidate the reasons for the improved bonding performance induced by the flow modifier at the submicron level.

An Al–5Sr–8Ce master alloy was fabricated as a novel modifier [46], and its effect on the microstructure and tensile properties of A356 alloy was systematically investigated. The solution treatment time was also optimised based on the modification efficiency of Al–5Sr–8Ce. The alloy was found to consist primarily of α-Al, Al_4Sr, and $Al_{11}Ce_3$ phases. Increasing the content of Al–5Sr–8Ce to 0.4 wt.% significantly reduced the grain size and the secondary dendrite arm spacing (SDAS), while transforming the eutectic Si morphology from lamellar to fine, rod-like structures. The refinement was primarily attributed to the retardation of grain growth due to Ce segregation and the formation of Ce-containing intermetallics at grain boundaries. The superior modification effect was ascribed to the synergistic enhancement of Sr modification and suppression of eutectic Si growth by Ce. Multiple levels of microstructural refinement by Al–5Sr–8Ce improved the grain boundary interconnectivity, which was the main contributor to grain refinement.

The microstructural evolution and mechanical properties of Al–7Si–0.35Mg alloy with different amounts of submicron-sized TiC particles were investigated in Ref. [47]. The results showed that the addition of TiC decreased the critical undercooling for α-Al nucleation and reduced the size of secondary dendrite arms and eutectic phase grains, while the lamellar Si phase adopted a fibrous morphology. As the TiC content increased, the mechanical properties of the aged composites initially improved and then deteriorated. The composite containing 0.3 wt.% TiC exhibited the optimal combination of mechanical properties, with tensile strength, 0.2% yield strength, and elongation increasing from 293 MPa, 220 MPa, and 7.7% to 315 MPa, 240 MPa, and 16.3%, respectively. This improvement was mainly attributed to microstructural refinement and modification of the Si phase due to the appropriate addition of TiC. In contrast, excessive TiC content led to particle agglomeration and the formation of coarse undissolved Al–Mg–Si–Fe phases and needle-shaped Al–Si–Ti intermetallic compounds, which reduced both ductility and strength.

Despite the many advantages of Al–Si alloys, their industrial application remains limited by their low ductility, which is due to the presence of lamellar Si particles embedded in the aluminium matrix. The effect of sodium modification on the microstructure and mechanical properties of hypoeutectic Al–Si alloys was examined in Ref. [48]. Modification was carried out using pure Na at concentrations of 0.08, 0.12, and 0.16 wt.% with holding times of 10, 15, and 20 minutes. The microstructures of the modified samples were analysed by optical microscopy, and the eutectic particle size was measured using ImageJ software. In all cases, the modified microstructure exhibited fine, fibrous eutectic Si particles uniformly distributed throughout the matrix.

The microstructural role of TiB addition in the modification of eutectoid Zn–Al alloy (ZA27) was investigated in Ref. [49] using scanning electron microscopy, high-angle annular dark-field scanning transmission electron microscopy, and energy-dispersive X-ray spectroscopy. A series of Zn–27Al–2Cu–0.02Mg–x(Ti + B) alloys ($x = 0$, 0.01, 0.02, 0.05, 0.10, 0.20 wt.%) were cast. The results demonstrated that the hardness and strength of the ZA27 alloy increased with rising (Ti + B) content, peaking at 0.05 wt.%. The TiB modifier refined the primary α-Al grains and altered the coralloid eutectoid (α-Al + η-Zn) microstructure, which was responsible for the improved mechanical properties. The modified eutectoid exhibited distinctive basket-shaped and ribbon-shaped morphologies. The enlargement of the primary α-Al grains was attributed to constitutional undercooling caused by B segregation at the solid–liquid interface. The participation of B and/or Ti in eutectic and eutectoid reactions also contributed to changes in the morphology of the eutectoid structure.

In Ref. [50], a systematic review was conducted to evaluate the effects of various alloying elements (including boron, carbon, chromium, manganese, molybdenum, niobium, rare-earth elements, silicon, titanium, and vanadium) on the wear resistance of iron-based alloy coatings.

Spheroidal graphite cast irons (SGCIs) are widely used in the automotive and power generation industries where high mechanical strength and wear resistance are essential. The aim of the study [51] was to investigate the effect of vanadium content and cooling rate on the performance of these alloys. SGCIs alloyed with varying vanadium contents (0, 0.25, 0.5 and 1 wt.%) were produced with different cross-sectional sizes (10, 20, 30, 40, and 50 mm) by sand casting. Microstructural evaluation revealed that the density of V_8C_7 carbides and the pearlite fraction increased, while the ferrite fraction decreased, with increasing vanadium content and decreasing section size. The quantity of graphite particles was found to be inversely proportional to carbide deposition: greater carbide formation resulted in larger, less spherical graphite nodules. Castings with thinner walls, providing higher cooling rates, exhibited superior mechanical strength. Minimum wear loss was achieved in SGCIs with 0.5 wt.% vanadium across all section sizes. In contrast, a vanadium content of 1 wt.% significantly reduced impact toughness due to excessive carbide density, resulting in lower wear resistance despite higher strength.

Two types of alloyed nodular cast iron were produced by induction melting and sand mould casting [52]. The first alloy was alloyed with 4 wt.% silicon and 1 wt.% molybdenum (EN-GJS-X300SiMo4-1), and the second with 4 wt.% silicon and 1.5 wt.% copper (EN-GJS-X300SiCu4-1.5). The microstructures of the samples were examined by optical metallography. The addition of molybdenum promoted ferrite formation and slightly increased graphite nodule size, while decreasing their number. Conversely, copper addition promoted pearlite formation, reduced graphite size, and increased the number of nodules. Mechanical properties were evaluated by tensile, impact bending, and Brinell hardness tests.

The microstructure and abrasion resistance of a wear-resistant steel developed using the CALPHAD approach were characterised and evaluated in Ref. [53]. This steel demonstrated significant advantages over conventional high-chromium cast iron due to the precipitation of micron-sized M_7C_3 carbides from austenite *via* a disorientation transformation, yielding a more uniform distribution with desirable size and shape. Additionally, the steel incorporated micron-sized carbides (M_7C_3, VC and Mo_2C) and submicron-sized carbides (M_7C_3 and VC) as hardening phases, while nanoscale carbides (Mo_2C, M_7C_3 and M_3C) contributed to dispersion strengthening.

The wear and impact–abrasion resistance of the steel were 1.8 and 1.7 times higher, respectively, than those of KmTBCr26 under identical wear conditions. These findings indicate that the modified micron-sized M_7C_3 carbides effectively suppressed undesirable phenomena such as cracking and chipping during wear, resulting in improved impact–abrasive wear resistance.

A significant challenge in producing TiC-reinforced metal matrix composites lies in the direct addition of TiC particles into molten steel during casting, as nanoscale TiC particles tend to float and agglomerate. In Ref. [54], a novel strategy was proposed involving *in situ* pre-distribution of nanoscale TiC/Al ligatures in the casting process, effectively mitigating this issue. In cast and heat-treated 45 steel with 0.018 wt.% TiC nanoparticles, the average grain size decreased significantly, from 14.75 μm to 9.51 μm and further to 8.77 μm and 5.46 μm, respectively, attributed to the provision of effective nucleation sites and inhibition of grain growth by the nanoparticles. Moreover, TiC nanoparticle addition substantially improved strength and toughness. Composites of steel 45 reinforced with 0.054 wt.% TiC nanoparticles exhibited optimal tensile properties: yield strength of 624 MPa, ultimate tensile strength of 920 MPa, elongation of 23.8%, and impact toughness of 0.50 J/cmI — improvements of 19%, 13%, 10%, and 38%, respectively, over conventional steel 45. The hardening mechanisms of nanoscale TiC were identified as grain boundary strengthening, strain hardening, and dispersion strengthening.

The effects of individual and combined additions of La and Ce on the microstructure, thermal conductivity, and mechanical properties of Al–3Si–0.5Cu–0.7Fe cast alloys were investigated using optical microscopy, scanning electron microscopy, and tensile testing [55]. The results showed that rare earth element additions (La and Ce) improved the microstructure significantly. In the Al–3Si–0.5Cu–0.7Fe–0.3(La + Ce) alloy, the secondary dendrite arm spacing decreased by 41.2%, reaching its minimum value. Additionally, the average area and aspect ratio of the eutectic silicon phase were decreased by 72.7% and 81.7%, respectively. The alloy modified with 0.3 wt.% (La + Ce) also exhibited the highest thermal conductivity (176.33 W/m·K), attributed primarily to the refinement and morphological modification of the eutectic silicon phase.

Silicon significantly influences the formation of carbides and the nanobainitic structure, thereby enhancing the wear resistance of alloys [56]. To elucidate the effect of silicon content on the microstructure and wear resistance of high-vanadium wear-resistant alloys (HVWAs), three silicon levels (0.66%, 2.14%, and 5.17%) were added to HVWAs, and a nanobainitic matrix was obtained by isothermal quenching at low temperature. Vanadium carbides (VC) were distributed within the nanobainitic matrix. With increasing silicon content, the proportion of VC in the form of granules or agglomerates increased, while the proportion of VC in banded or chrysanthemum-like morphologies decreased. The thickness of bainitic ferrite bands and the thin film of retained austenite gradually decreased with increasing silicon content, with bainitic-ferrite band thicknesses of 100–600 nm, 50–450 nm and 50–350 nm for the three alloys, respectively. The alloy containing 2.14% silicon exhibited excellent combined mechanical properties and wear resistance. Compared with the other two alloys, the impact toughness of the 2.14% Si alloy improved by 10.2% and 151.8%, while wear weight loss decreased by 35.4% and 60.1% under a wear load of 2.387 MPa and abrasive size of 48 μm. Owing to the increased presence of high-hardness VC particles and the significantly refined nanobainitic matrix, which effectively resists abrasive damage, the alloy with 2.14% silicon demonstrated outstanding strength and wear resistance.

The use of secondary aluminium casting alloys with high iron content in the production of automotive structural components is limited due to their low ductility, arising from various intermetallic phases that form during solidification. In Ref. [57], the effect of cerium on secondary cast Al–Si–Mg–Fe alloys was systematically studied using thermodynamic modelling and experimental analysis. Thermal analysis and microstructural observations were compared with thermodynamic predictions. Transmission electron microscopy (TEM) confirmed the presence of $MgAl_2Si_2$, Al_2CeSi_2, AlCeSi, and $AlCeSi_2$ phases as a function of Ce content, as well as π-$Al_9FeMg_3Si_5$ and δ-Al_3FeSi_2. Adding 0.25–0.5 wt.% Ce increased the relative elongation at fracture by approximately 40%, exceeding 5%. The Al–Si–Mg–Fe–0.25Ce alloy exhibited the highest relative elongation (5.2%) and tensile strength (234 MPa) due to the suppression of π-$Al_9FeMg_3Si_5$ and Mg_2Si phases, which were absorbed by the Ce additions. These additions up to 1 wt.% only slightly modified the eutectic Si and did not significantly affect the secondary dendrite arm spacing or the morphology of Fe-containing primary intermetallic phases. Excessive Ce content, however, led to the formation of large Ce-containing intermetallics, which negatively influenced ductility.

Rare earth elements (REEs) are known to be excellent modifiers of non-metallic inclusions, which inevitably form in steel and adversely affect its properties [58]. This study reviewed the state of research on inclusion modification by REEs and its effect on steel properties. The sequence of inclusion evolution following RE addition was summarised as follows: $M \rightarrow M + \mathrm{RE{-}Al{-}O} \rightarrow \mathrm{RE{-}Al{-}O} + \mathrm{RE_2O_2S} \rightarrow \mathrm{RE_2O_2S} + \mathrm{RE{-}S/RE_2O_2S} + \mathrm{RE{-}O}$, where M denotes the original inclusions before RE addition. The final type of inclusions after RE modification depends on the relative sulphur and oxygen content of the steel. Appropriate amounts of RE additions can produce fine, regular, and uniformly distributed inclusions.

During the final stages of solidification, γ-austenite forms. Changes in the size and number of primary carbides are associated with the segrega-

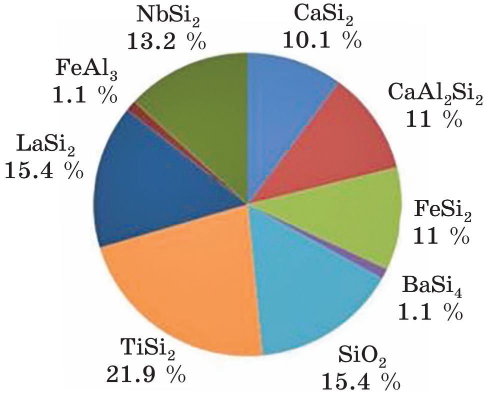

Fig. 1. Representative fragments of the INSTEEL-class modifier used for alloy modification (*a*) and phase composition analysis results (*b*) [60]

tion of residual melt into separate γ-austenite grains, with Ce atoms accumulating at grain boundaries and contributing to grain refinement [59]. Thermodynamic calculations showed that primary carbides, precipitating *via* heterogeneous nucleation of C-carbides in the intergranular regions, became more refined, with their volume fraction decreasing from 4.15% to 2.1%. The role of Ce inclusions was investigated using combined experimental and theoretical methods. When a small amount of cerium (0.056 wt.%) was added, large columnar grains in the as-cast microstructure were transformed into equiaxed grains, and the average grain diameter decreased from 56 μm to 27 μm.

In the study [60], the steel grade 40CrNi3MoV was used as the research material, with the complex INSTEEL nanomodifier (Fig. 1) employed as the modifier. This nanomodifier is distinguished by its complex composition, which includes alkaline earth metals, rare earth elements (REEs), and the strong carbide-forming element titanium. It was established that the introduction of this modifier improves the steel's properties, including ultimate tensile strength, hardness, impact toughness, and wear resistance.

Figure 2 shows the microstructures of the samples without the nanomodifier (sample 1) and after the introduction of the nanomodifier (sample 2).

Chemical composition at selected points of the sample (see spectra 90 and 119 in Fig. 2) [60]

Spectrum	C	Si	Ti	Cr	Mn	Ca	Ba	Ni	Al	La	Mo	Fe
Spectrum 90	0.35	1.3	0.03	1.36	0.35	—	—	3.68	—	—	0.38	bal
Spectrum 119	0.31	1.2	0.15	1.40	0.43	0.68	0.35	3.63	0.07	traces	0.37	bal

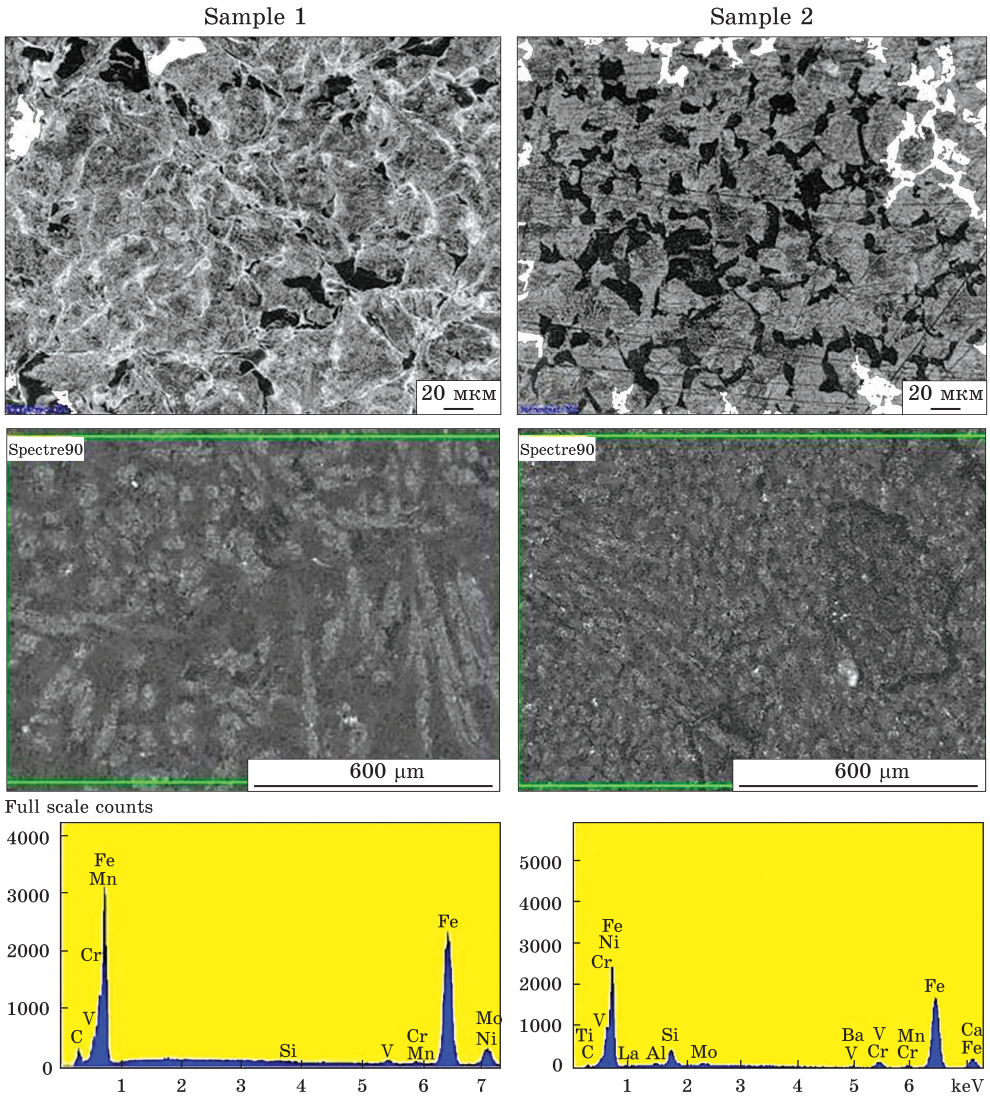

Fig. 2. Microstructural characterisation and spectral analysis of 40CrNi3MoV steel before modification (*a*) and after the addition of the INSTEEL nanomodifier (*b*) [60]

Table presents the results of the overall elemental composition (spectra 90 and 119, Fig. 2).

A comparison of the microstructures demonstrates that, after the addition of the nanomodifier, sample 2 exhibits a more refined and homogeneous structure, which is expected to contribute to improved fundamental mechanical properties, such as hardness, strength, and others.

According to metallographic analysis [61], the initial surface structure was ferrite–pearlite. After plasma treatment, a transformation was obser-

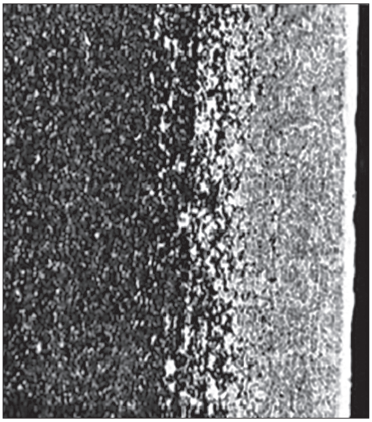

Fig. 3. Microstructure of the sample surface after modification (magnification ×100) [61]

ved on the surface into a fine-needle martensitic structure, while a sorbitic pearlite-like structure formed in the core of the sample (Fig. 3).

Thus, it can be determined that the most commonly used modifiers are rare earth metals and metal carbides with high melting points. Several studies have examined the combined effect of modifiers with external influences, such as ultrasonic vibrations.

3. Use of Mechanical Effects in the Production of Alloys (External Effects)

Despite their lightweight and high-temperature resistance, TiAl alloys exhibit limited thermoplastic formability, which significantly restricts their application in complex structural components for the aerospace industry. To enhance the thermoplastic formability of TiAl alloys while maintaining their performance characteristics, a study [62] applied a forming technique assisted by mechanical vibration and developed a dedicated platform for vibration-assisted tensile testing. In the vibration tensile test (VT), low-frequency vibration at 1.5 Hz was applied, resulting in a peak stress of 194 MPa in the sample, which is approximately 21% lower than the 242 MPa observed in the conventional tensile test (NT). This study demonstrated for the first time that vibration-assisted mechanical forming technology could significantly reduce stress during the forming of TiAl alloys. Further results showed that vibration enhanced the ability of dislocations to glide over long distances and promoted their rearrangement and annihilation, which significantly improved the dynamic recrystallization (DRX) capability.

In mechanical engineering, particularly in the automotive and aerospace sectors, magnesium alloys are increasingly utilised due to their high strength-to-weight ratio. However, their surface properties often require enhancement to meet the demands of high-performance applications. Study [63] evaluated the mechanical and tribological properties of AZ31/$CeO_2 + h$BN hybrid surface composites fabricated *via* friction stir processing (FSP) and vibration-assisted friction stir processing (VAFSP). The VAFSP method significantly reduced the average grain size to 5.19 µm, compared to 7.25 µm in FSP-treated samples. Furthermore, VAFSP-treated samples exhibited a 15% increase in hardness and a more uniform distribution of reinforcing particles throughout the matrix. The results also showed that the shear punch strength (SPS) of VAFSP-treated samples reached 178 MPa. Tribological testing revealed that the wear rate of VAFSP-treated samples was 40% lower, demonstrating the potential of VAFSP as an effective technique for surface composite fabrication of AZ31 alloy reinforced with CeO_2 and *h*BN.

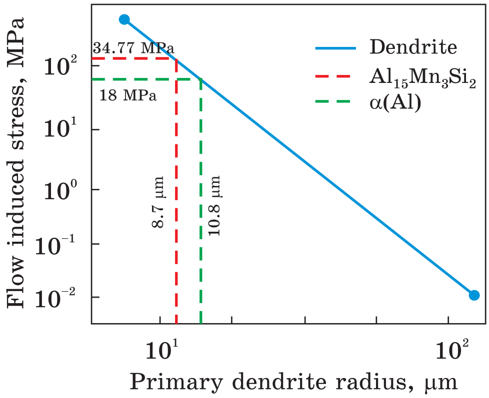

Fig. 4. Effect of the acoustic energy flow on the α-Al and $Al_{15}Mn_3Si_2$ dendrites [64]

The effects of ultrasonic vibration (UV) and mechanical vibration (MV) on the modification of the manganese-rich phase and mechanical properties of Al–12Si–4Cu–1Ni–1Mg–2Mn piston alloys were investigated in [64]. The results indicated that both UV and combined UV + MV treatment significantly refined and fragmented the microstructure. Additionally, UV treatment was shown to passivate effectively the primary manganese-rich $Al_{15}Mn_3Si_2$ intermetallics. The mechanisms of grain refinement and passivation of non-deuteride particles were discussed. Compared to conventional die-cast alloys, alloys treated with UV and UV+MV demonstrated enhanced tensile strength and creep resistance at both room and elevated temperatures. These improvements were attributed to the refinement of α-Al grains and secondary intermetallic phases, an increased proportion of refined heat-resistant precipitates, and the formation of nanoscale Si particles. Notably, the tensile strength of UV-treated alloys at 350 °C exceeded that of commercial piston alloys, underscoring the high potential of these developed piston alloys for use in high-performance diesel engines.

Figure 4 illustrates the mechanical stress induced in the α-Al and $Al_{15}Mn_3Si_2$ dendrites by the influence of the acoustic energy flow.

The image processing and segmentation procedures are illustrated in Fig. 4. X-ray diffraction (XRD) analysis was carried out using a Bruker AXS D8 ADVANCE diffractometer (Karlsruhe, Germany) to investigate the phase evolution under different casting conditions. The precipitate particles in the α-Al matrix were examined by transmission electron microscopy (TEM; JEOL JEM-F200, Japan) operated at 200 kV.

The use of fins and external fields has been considered an effective approach to enhancing heat transfer efficiency in phase change materials (PCMs). However, the combined influence of mechanical vibration and fin structures on heat transfer characteristics has not been extensively studied. In Ref. [65], numerical modelling was performed to investigate the effects of mechanical vibration and fin structures on the melting behaviour of PCMs. It was found that the enhancement of heat transfer due to fins and mechanical vibration was primarily associated with improved convective heat transfer and thermal conductivity. The results showed that the total melting time of PCMs subjected to vertical vibrations of π and 3π and horizontal vibrations of π increased by 5.6%, 4.3%, and 2.4%, respectively. Conversely, PCMs subjected to vertical vibration of 5π and horizontal vibrations of 3π and 5π exhibited reduced melting times by 16.78%, 10.5%, and 8.4%, respectively, compared to PCMs without vibration. These findings demonstrated that the interaction between ribbed structures and mechanical vibration could exert both enhancing and inhibiting effects on heat transfer, exhibiting a mutually limiting relationship between the two factors.

The NiCoCr multi-principal element alloy (MPEA) exhibits excellent plasticity at cryogenic temperatures and corrosion resistance, provided it be produced *via* thermomechanical processing [66]. However, the presence of large grains in the as-cast state significantly impairs its mechanical properties, necessitating grain refinement to produce complex castings. Most grain-refinement techniques require additional alloying elements, which can reduce ductility due to the formation of brittle secondary phases. In this study, a significant improvement in the microstructure of as-cast NiCoCr MPEA was achieved by applying mechanical vibration in vacuum conditions to avoid contamination. The average grain size was reduced from 620 μm to 140 μm. As a result, the yield strength at room temperature increased by 54% (from 255 MPa to 392 MPa) without compromising ductility compared to the non-vibrated as-cast alloy.

Study [67] investigated the effect of vibration frequency on the physical and mechanical properties and residual stresses during welding of dissimilar metals AA5083 and AA6061. The vibration welding process was conducted at frequencies of 0, 10, 30, and 50 Hz. The resulting welds were evaluated for microstructure, tensile strength, and impact toughness, while surface residual stresses were measured *via* x-ray diffraction. The results showed that welding at a vibration frequency of 50 Hz produced a fine-grained, homogeneous, equiaxed microstructure with exceptional mechanical properties: ultimate tensile strength of 197.87 MPa, elongation of 15.28%, and impact toughness of 8.10 J. Moreover, this weld exhibited the lowest residual surface stress in the weld metal, at 110.9 MPa. The application of high-frequency vibrations during aluminium welding improved the uniform mixing of molten AA5083 and AA6061 and increased internal pressure in the weld pool, facilitating the escape of dissolved gases (H_2, O_2, N_2) as bubbles.

Article [68] examined the influence of microstructure and impact toughness of Q450NQR1 steel welded joints, exposed to atmospheric corrosion, on low-frequency mechanical vibrations during gas metal arc welding (GMAW). The cooling and solidification processes of the molten metal during vibration welding were analysed using a one-dimensional Stefan problem and a model based on the wave equation. The calculations showed that increasing vibration frequency reduced the cooling time of the molten metal and increased the stress within dendrites during solidification. Mechanical vibrations with fixed amplitude of 0.1 mm and frequencies of 0, 20, 40 and 60 Hz were applied to the weld pool under identical welding parameters.

Results from molecular dynamics (MD) simulations [69] revealed that microstructure and vibrational parameters significantly influence the imprinting load, elastic recovery coefficient, and deformation behaviour of the FeNiCrCoCu high-entropy alloy (HEA). The imprinting force curve demonstrated that the maximum loading force decreased in the following order: monocrystalline, nanotwinned (NT) polycrystalline, and polycrystalline structures. In the polycrystalline structure, a reverse Hall–Petch relationship was observed as the grain size varied from 5.1 nm to 9.8 nm. Grain boundaries (GBs) were identified as key contributors to strengthening, with grain splitting, GB migration, and grain rotation being the primary deformation mechanisms in this regime. In NT polycrystals, stability was enhanced by twin boundaries (TBs), and TB migration near the imprint region was examined.

Reference [70] described a mechanical vibration technique to improve crystalline structures by introducing vibrational energy directly into molten Al–5 wt.% Cu alloy using a vibrating horn that partially melted during operation. The effects of acceleration and mass ratio on the alloy's microstructure were investigated. The results demonstrated that mechanical vibration could induce localised cooling by extracting heat from the molten interior, with the cooling rate strongly dependent on the vibration acceleration. However, significant grain refinement was difficult to achieve if the alloy remained fully liquid throughout the vibration period. Notable grain fragmentation was achieved when mechanical vibration was applied during the initial stages of solidification. The underlying grain refinement mechanisms were further discussed.

Research into phase-change materials (PCMs) for solar energy storage aims to store latent heat over periods of days or even months. The authors of Ref. [71] confirmed the persistent supercooling behaviour of a xylitol/erythritol eutectic mixture. To initiate crystallisation and trigger heat release on demand, they proposed a combined method of mechanical stirring with seeding. The xylitol/erythritol eutectic was shown to remain supercooled without crystallisation at ambient temperature for at least 10 days, making it a suitable PCM for controlled heat release. This pronounced supercooling was attributed primarily to the unique molecular structure of the polyols and the marked increase in dynamic viscosity.

Mechanical vibration has also been employed to enhance the mechanical properties of wire-arc additive-manufactured (WAAM) 2319 aluminium alloy, addressing issues related to coarse grains and porosity [72]. The study aimed to investigate the influence of different vibration acce-

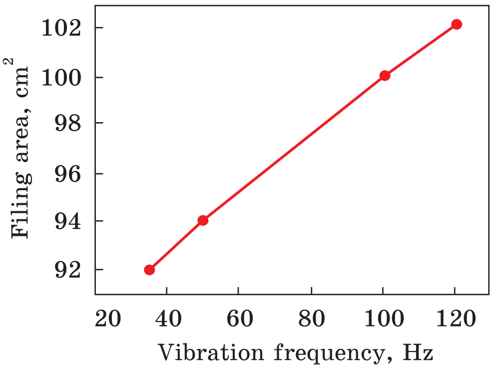

Fig. 5. Effect of mechanical vibration parameters on the solidification of the AZ91D alloy [73]

lerations on the microstructure and mechanical properties of the specimens. The authors proposed a mechanism in which solute redistribution under vibration significantly improved ductility. Vibration disrupted dendritic growth, leading to grain refinement. Solutes from interdendritic regions were redistributed into the liquid phase, reducing their concentration in these regions. A previously continuous, coarse-grained precipitate phase became discontinuous and fine-grained, thereby enhancing the ductility of the matrix.

Mechanical vibration induces relative motion between the liquid and solid phases during solidification, promoting dendrite fragmentation, which refines grains and increases equiaxiality. This benefits casting quality and overall mechanical performance. Article [73] investigated the influence of vibration parameters (in combination with EPC) on the filling ability, microstructure, and properties of AZ91D alloy.

Figure 5 presents the macromorphology and quantitative indices of AZ91D alloy filling under various vibration frequencies and fixed amplitude of 1 mm. The pouring temperature was 725 °C.

Figure 6 presents statistical data on the length, width, and aspect ratio of the secondary phase in AZ91D alloy under different mechanical vibration frequencies. It is evident that with increasing vibration frequency, the length and width of the secondary phase initially decrease and then increase.

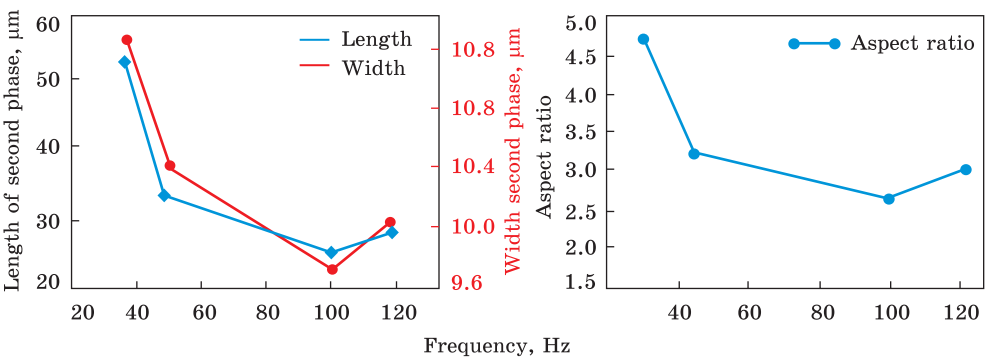

Fig. 6. Effect of mechanical vibration frequency on the formation of the second phase in the AZ91D alloy [73]

In line with the 'zero-defect' approach aimed at eliminating internal defects in castings and improving mechanical properties [74], gravity die-casting remains one of the most advanced continuous casting processes for non-ferrous alloys such as LM25 aluminium alloy. Mould vibration during casting is a novel technique to reduce internal defects such as porosity, gas entrapment, and shrinkage. In this experimental study, LM25 alloy was melted in a resistance furnace. Vibration was applied to a graphite mould using an electromechanical exciter during pouring and solidification. Vibration frequencies of 20, 25, 30, 35, 50 and 100 Hz at constant amplitude of 0.5 mm were tested; a non-vibrated (0 Hz) sample served as a reference. Both vibrated and non-vibrated samples were evaluated by hardness, tensile strength, elongation, yield stress, and microstructural morphology, analysed by scanning electron microscopy. The results showed that increasing vibration frequency led to a linear increase in hardness, increased yield strength at higher frequencies, reduced ductility, and significant grain refinement in an optimal frequency range of 30–35 Hz.

Study [75] reported the first application of mechanical vibration in lost-wax casting of A356 aluminium alloy, aiming to improve its microstructure and mechanical properties. The effect of wall thickness on microstructure and mechanical behaviour was also analysed. In Ref. [76], the effect of vibration frequency and duration on the primary α-Al phase size and density of A356 alloy was examined. Vibration frequencies of 10, 20, 30, 40 and 50 Hz and durations of 5, 10 and 15 minutes were tested. Vibration at 50 Hz for 15 minutes reduced the α-Al phase size by 53%, down to 173 μm, and achieved the highest density of 2.68 g/cm^2.

Phase-change materials (PCMs) play a crucial role in thermal energy storage systems, but their heat transfer performance remains a limitation. Prior studies explored active and passive methods to improve melting efficiency. Study [77] combined both approaches, investigating the effect of mechanical vibration on nanoparticle-reinforced PCMs in a horizontal 3*D* shell-and-tube thermal storage system. Phase change was modelled using the enthalpy–porosity method. Control equations were solved using finite volumes, with vibration forces incorporated *via* a user-defined function. Parameters included vibration frequency (ω), amplitude (*A*), and graphene nanoplatelet (GNP) concentration (φ). Results showed that at $\varphi = 5\%$, $A = 10$ mm, and $\omega = 500$ rad/s, the complete melting time decreased by ≅81.1% compared to no vibration. With $\varphi = 5\%$, $\omega = 100$ rad/s, and $A = 40$ mm, the melting accelerated by 50.3%. Combining maximum φ with high vibration reduced the melting time by 98.9%, while energy storage density increased nearly twelvefold within two minutes compared to static conditions. A 'resonance effect' at ω = 300 rad/s led to a rapid phase transition, which diminished at high GNP concentrations due to a damping effect.

Study [78] examined the influence of mechanical vibration during solidification on the metallurgical structure of hypoeutectic A356 Al–Si alloy. Castings were tested under varying vibration levels at different pouring temperatures and solid fractions. It was found that the average grain size of the primary Al phase decreased and became more equiaxed as vibration intensity increased, suggesting that vibration fragments dendrites more effectively at higher solid fractions (*i.e.*, lower pouring temperatures).

The behaviour of ZL205A castings under 'explosive feeding' with vibration and low pressure was investigated both experimentally and through physical modelling [79]. The results showed that vibration-assisted solidification under low pressure induced multiple explosive feeding events, creating shrinkage cavities with layered structures. Vibration-enabled mould filling with reduced shrinkage and higher density. The model indicated that explosive feeding occurs spontaneously with vibration but is difficult to achieve without it under low-pressure die-casting. Vibration eliminated bridging through pressure differentials, promoting grain mixing and preventing blockages.

Study [80] summarised the effect of low-frequency mechanical vibration on porosity in unmodified and sodium-modified LM25 (Al–Si 7.15%) and LM6 (Al–Si 12.30%) alloys. Vibration frequencies from 15 to 41.7 Hz and amplitudes of 0.125–0.5 mm were applied during solidification. Results showed that LM25 and LM6 modified with Nucleant2 exhibited reduced porosity volume, but porosity size and number increased in unmodified alloys with stronger vibration. Sodium modification reduced pore number but increased pore size compared to static conditions. Vibration at 31.7–41.7 Hz and amplitude 0.375–0.5 mm caused large pores at the top of unmodified and modified ingots.

Study [81] proposed an effective melt-cleaning method for A356 alloy, combining stirring and vacuum. The mechanisms of defect formation and their effect on mechanical properties were investigated. Compared to the untreated alloy, the cleaned A356 showed significantly improved mechanical performance. Cleaning parameters (stirring rate and temperature) influenced dendrite and pore size. Optimal conditions (65 rpm, 730 °C) yielded an average grain size of 279 μm and pore diameter of 79.5 μm; tensile strength reached 203.7±4.3 MPa, yield stress 81.6±3.3 MPa, and elongation 10.2±0.5%. The microstructural and mechanical improvements were attributed to bubble rupture mechanisms that accelerate degassing under vacuum stirring.

An analysis of the scientific literature confirms that the application of mechanical oscillations can significantly modify alloy microstructures. Oscillations can be applied to melts, solid-state alloys, or coatings, and are effective for both ferrous and non-ferrous alloys alike.

4. Use of Ultrasonic Oscillations and Electromagnetic Fields during Melt Crystallisation (External Effects)

Article [82] reviews recent advances in electromagnetic processing of metals to enhance material performance and outlines future directions. It examines the mechanisms of interaction between electromagnetic fields and metals (including both thermal and non-thermal effects) and provides a structured overview of how electromagnetic fields influence grain size, phase composition, dislocation density, and defect elimination. The article also summarises their effects on physical and mechanical properties such as tensile strength, fatigue resistance, wear resistance, corrosion resistance, impact toughness, and residual stress modification. Finally, the review highlights the significant potential of electromagnetic processing technologies for optimising metals across industrial applications, while also identifying current challenges and directions for future research.

Applying alternating current generates electromagnetic vibrational forces. Study [83] investigated the formation of grain structures in AZ31 magnesium alloys solidified under electromagnetic vibration at frequencies ranging from approximately 500 Hz to below 2000 Hz. Both extremely low and very high frequencies produced coarse-grained structures. In the viscous regime, the pronounced difference in electrical conductivity between the solid and liquid phases causes solid particles to move substantially faster than the surrounding fluid, resulting in relative displacement and dendrite fragmentation. This motion induces mixing at the semisolid stage, yielding a chaotic microstructure with deformation twins. At low frequencies, coarse structures may result from suppressed macrofluid flow due to strong magnetic fields. Grain refinement occurs within an intermediate frequency range, where the mobile solid vibrates beyond the solute boundary layer; at high frequencies, relative displacement is insufficient to disrupt boundary layers, leading to coarse structures similar to those formed during conventional casting.

Liquid metal (LM) is widely used in high-temperature thermal energy transfer and flow control, yet effective methods for controlling thermal-flow behaviour remain limited. Study [84] developed a compact integrated electromagnetic pump with a rotating permanent magnet (PM EMP) for liquid metal, accompanied by a three-dimensional multiphysics numerical model and precise analytical correlations. The results demonstrated that optimising electromagnetic parameters reduces nonsinusoidal current distributions, thereby improving output performance and flow stability. Enhancing tangential leakage currents increased vertical current density by 110%, suppressing edge effects and mitigating pressure pulsations, which improved the overall pump characteristics. The modified analytical correlation achieved an accuracy improvement of over 90% at 28.9%. Prototype experiments validated the theoretical predictions.

Liquid metal subjected to a moving magnetic field presents an effective tool for controlling phase-transition processes in metals. Article [85] presented numerical and experimental investigations of the electromagnetic forces generated by moving magnetic-field acting on liquid gallium, demonstrating control over flow and solidification/melting behaviours. A three-dimensional numerical model was developed to calculate the magnetic field and force distributions in a laboratory-scale rectangular cavity.

A review [86] summarised the state of the art in electron, ion-beam, and combined irradiation processing of titanium and its alloys. Such treatments enhance the physical and mechanical properties of titanium-based materials, with combined processes yielding significant property improvements.

A numerical study [87] examined the effects of standard vibrational electromagnetic field (VMF), differential-phase VMF, standard low-frequency electromagnetic field (LFMF), and differential-phase LFMF on the flow and structure of molten magnesium alloys (AZ31B and AZ80) under direct cooling (DC). Based on the theory of thermal crystal growth, the study explored the relationships between velocity fields, temperature fields, and solidification structures. Experimental low-pressure die-casting confirmed the theoretical predictions.

In directional solidification, the combination of intense shear flow and a magnetic field was shown to refine significantly grains in ingots [88]. Understanding the changes in flow and temperature distributions under combined fields is crucial for elucidating the mechanisms of grain refinement.

Work [89] asserts that the development of materials with ultrafine-grained structures remains a central objective in materials science and highlights the promise of external processing techniques for achieving such structures without altering chemical or phase composition.

Study [90] reports the first casting of the $Al_{70}Zn_{10}Mg_{10}Cu_5Si_5$ medium-entropy alloy using electromagnetic stirring. This process had minimal effect on phase formation, which in cast alloys primarily consists of α-Al solid solution, Mg_2Si, Al_2Cu and $MgZn_2$ phases. The size of Si particles decreased from 40.0 μm to 17.7 μm.

Uniform dispersion of the Sn phase in Al–Sn alloys improves their properties, but metastable miscibility gaps cause macrosegregation in conventional casting. Study [91] solidified an Al–20% Sn–1% Cu alloy under a static magnetic field combined with current-induced electromagnetic vibration (EMV). At a vibration frequency of 100 Hz, the Sn phase was refined and uniformly dispersed within the primary Al matrix, in contrast to the continuous Sn networks observed in static casting.

The mechanical properties of aluminium castings are strongly dependent on hydrogen-related porosity. Ultrasonic treatment is an effective method for both modifying the structure and degassing aluminium alloys. However, the transmission of ultrasonic waves through moulds is inefficient on an industrial scale. Study [92] aimed to develop reliable ultrasonic equipment capable of delivering sufficient power into molten metal and achieving an optimal acoustic field distribution during solidification.

Study [93] examined hypoeutectic Al–7% Si and hypereutectic Al–17% Si alloys solidified under electromagnetic stirring (EMS). Microstructural changes were assessed as a function of EMS exposure time. Both primary α-Al in Al–7% Si and primary Si in Al–17% Si were refined with sufficient EMS. In addition to induced flow, a novel mechanism was proposed to explain grain refinement, based on significant conductivity differences between the primary solid and remaining liquid.

Ultrasonic vibration (UVT), as an auxiliary method, enables improved control over microstructure and porosity in cast components. Study [94] developed a thermal exchange model and conducted in situ high-speed visualisation experiments under various process parameters. UVT enlarged the melt pool, achieved more uniform temperature distribution, and significantly refined the grains. Frequency and amplitude directly influenced melt flow behaviour, reducing porosity by 64% and decreasing pore diameter from 45 μm to 18 μm.

The primary aim of study [95] was to evaluate the effects of external physical fields on the microstructure and mechanical properties of ultra-rapidly solidified Al–Mg–Si alloy. Microstructural evolution, compositional distribution, hardness, and tensile properties of cast and rolled strips were thoroughly investigated using optical microscopy (OM), electron probe microanalysis (EPMA), tensile and hardness testing. Under external fields, α-Al became equiaxed and fine-grained, and the fraction of non-equilibrium eutectic phases decreased significantly. The most pronounced improvements were observed under electromagnetic oscillatory fields. Residual magnetic retardation and shock-wave effects from static magnetic fields and pulsed currents improved microstructural homogeneity, compositional uniformity, mixing, and solid-solution strengthening of the matrix.

Study [96] evaluated the effect of ultrasonic treatment on the microstructural features and tensile strength of AZ91 magnesium alloy. The melt was treated ultrasonically (approximately 20 kHz, 600 W) for five minutes before casting into sand moulds. Ultrasonic treatment significantly influenced the size and morphology of primary α-Mg dendrites, as well as the size, cohesion, sphericity, and distribution of intermetallic particles. Increasing ultrasonic power reduced grain size and roundness while producing more uniformly distributed particles. These microstructural changes are primarily attributed to cavitation and acoustic streaming during ultrasonic treatment. Tensile strength improved significantly after treatment, due to the refined and homogenised $Mg_{17}Al_{12}$ particles.

To enhance mechanical properties and ductility, a large refined equiaxed zone was generated in high-purity zinc using ultrasonic treatment [97]. The macrostructure of cast slugs transformed from coarse columnar grains into three zones: fine columnar, refined equiaxed core, and a mixed coarse/columnar zone. A small equiaxed zone formed when cooling from 440 °C to 419 °C over two minutes. This equiaxed zone expanded from ≈20% to ≈50% of the cross-sectional area when cooling was extended to 3–4 minutes. Conversely, ultrasonic treatment at higher temperatures or longer times (450 → 419 °C over four minutes) reduced the equiaxed zone by 18%, indicating that optimal time and temperature conditions are required for maximum equiaxed zone formation during solidification. Factors influencing equiaxed-zone formation throughout the cycle were described.

Study [98] investigated the effects of alternating and static magnetic fields during the casting of AZ80 magnesium ingots under direct current. Both fields were varied from 0 to 20 000 ampere-turns, with the alternating field frequency ranging from 0 to 30 kHz. It was found that electromagnetic vibrational forces refined the grains in AZ80 ingots: increasing the intensity of both fields further refined the grains by increasing nucleation sites and detaching dendrite arms. At an alternating field frequency of 30 kHz, the microstructure was greatly refined.

Eutectic Al–12.6% Si (by mass) typically forms fine Si platelets or rods within an Al matrix upon solidification. Directed solidification alone is insufficient to separate Al and Si in this eutectic structure. Study [99] developed a novel process to separate aluminium and silicon from the eutectic melt by applying directional electromagnetic separation forces at the solid–liquid interface during continuous casting. Analysis of the solidified structure confirmed effective separation.

Identifying the dominant mechanisms of grain refinement has been the focus of many studies, given the wide variation in processing conditions and external treatments [100]. Fine grains arise through heterogeneous nucleation or a combination of nucleation with dendrite and grain fragmentation, detaching from mould walls or the melt surface under vibration or stirring. The first part of this review describes the main external processing methods and grain-refinement mechanisms, while the second part critically compares current understanding to highlight differences, similarities, and factors promoting the formation of large equiaxed regions.

For most alloys, columnar grains lead to casting defects and mechanical anisotropy, making the transition to equiaxed grains and control of segregation critical in metallurgy. In study [101], the influence of convection induced by electromagnetic oscillation frequency on directional solidification structure in Al–15 Sn–1 Cu alloys was examined. Experimental results showed that reducing the electromagnetic oscillation frequency from 100 Hz to 1 Hz gradually changed the solidification front from inclined to flat. Furthermore, the number of equiaxed grains increased with decreasing frequency, culminating in a fully equiaxed structure at 1 Hz. Numerical simulations indicated that a flat solidification front resulted from a more uniform solute distribution and temperature oscillations.

The UVT, a highly effective method for dispersing second-phase particles in molten metals, was applied *in situ* to PRCMC composites using SiAlON. This study conducted systematic experiments on the effects of UVT on the microstructure and mechanical properties of *in situ* Cu–TiB composites. Results [102] indicated that the optimal UVT duration was 3 minutes, yielding improved TiB_2 particle dispersion and enhanced mechanical properties of the cast composite. Tensile strength, yield strength, and elongation increased by 15.7%, 18.1% and 36.1%, respectively, compared to the as-cast Cu–TiB_2 composite without UVT. These composites were subsequently subjected to rolling deformation, confirming that the Cu–TiB_2 composite treated with 3 minutes of UVT exhibited the best performance. The hot-rolled Cu–TiB_2 composite achieved an ultimate tensile strength of 459 MPa, yield strength of 422 MPa, and elongation of 7.0%.

The influence of electromagnetic oscillations (EMO) on the solidification structure of Cu–15 Ni–8 Sn alloy during bulk solidification and upward continuous casting was investigated experimentally and numerically. Bulk solidification results [103] demonstrated that at a magnetic flux density of 0.5 T and a current density of $1.27\cdot10^5$ A/mI, the most effective grain refinement occurred at an oscillation frequency of 10 Hz, producing fine, non-dendritic grains. By contrast, coarser solidification structures formed at 0.1 Hz and 1 Hz compared to 10 Hz, while no refinement was observed at 100 Hz.

To enhance the interfacial microstructure and bonding at the Al/Mg interface in composite mould casting, a hybrid process combining Gd alloying and ultrasonic vibration was applied. The interfacial microstructure, mechanical properties, and strengthening mechanisms at the Al/Mg interface under hybrid treatment were studied [104]. It was observed that the oxide film between the intermetallic compound (IMC) layer and the eutectic layer at the Al/Mg interface partially dissolved upon the addition of 0.6 wt.% Gd.

The effect of ultrasonic waves (20 kHz) on the dendritic structure of Sn–13 at.% Bi alloys was investigated *via* time-resolved *in situ* x-ray visualisation [105]. Sequential imaging revealed secondary phenomena such as ultrasonic streaming and low-frequency oscillations compared to the 20 kHz ultrasonic frequency. The ultrasonic waves induced circulating convection nearly equal to the sample size, along with periodic convection (≈40 Hz), evident in longitudinal dendrite oscillations. Fragmentation of primary and secondary dendrite arms in the columnar zone was significantly enhanced under ultrasonic treatment.

In Ref. [106], fixed-frequency ultrasonic field (FUF), low-frequency electromagnetic field (LEF), variable-frequency ultrasonic field (VUF), and combined VUF + LEF were applied during semi-continuous casting of AZ80 magnesium alloy to improve microstructure and mechanical properties. All external field treatments refined the grains, with the combined

VUF + LEF treatment producing the most pronounced reduction from 679–1454 μm (without treatment) down to 116–141 μm.

Study [107] explored the influence of low-frequency electromagnetic (LF-EM) and ultrasonic (US) fields on the microstructure, macrosegregation of alloying elements, and mechanical properties of cast AZ80 alloy. Both LF-EM and US fields refined the grains in ingots, improving mechanical properties and homogenising the distribution of alloying elements. Under LF-EM, grain refinement was more evident at the edges of the ingot, whereas ultrasonic treatment primarily refined the core. Combining LF-EM and US effects enabled the development of a novel direct-cooling–electromagnetic–ultrasonic casting (DC-ECUS) process for magnesium alloys, producing finer, more homogeneous grains throughout the ingot and enhancing mechanical performance.

High-intensity ultrasonic oscillations applied to liquid or semi-solid metals during solidification have attracted considerable interest from both researchers and industry. Ultrasonic melt treatment (UMT) produces significant improvements in structure, including grain and primary particle refinement, enhanced chemical and structural homogeneity, and reduced porosity [108].

Cast rods of AlSi7Mg alloy, produced *via* low-pressure casting, were subjected to ultrasonic treatment during cooling [109]. Microstructure and mechanical properties were characterised at various distances from the acoustic source, with a pouring temperature of 650 °C. This combined method produced castings free of gas porosity and solidification defects, promoted the formation of fine spheroidal α-Al grains, modified the Si eutectic, and refined and dispersed intermetallic phases. Mechanical properties (tensile strength, yield strength, and ductility) were correspondingly improved.

A numerical and experimental study [110] assessed the feasibility and efficiency of using standing ultrasonic waves to clean magnesium alloy melts. Numerical modelling addressed two aspects: wave propagation in various cell geometries was simulated to optimise the formation of standing waves, and the behaviour of oxide inclusions under these waves was analysed. It was predicted that oxide inclusions, whose apparent density is close to that of the melt, rapidly agglomerate at nodal points, thereby accelerating and enhancing their removal from the magnesium alloy melt.

Ultrasonic vibration was applied to the melt of Mg–8Li–3Al during solidification. The resulting microstructure, corrosion resistance, and mechanical properties were investigated [111]. The results indicated that ultrasonic vibration changed the morphology of the α-phase from coarse rosettes to fine globular grains. The finest globular structure was obtained at a power of 170 W, with refinement improving as treatment duration increased. Corrosion resistance of the alloy treated at 170 W for 90 s was markedly improved compared to the untreated alloy. Mechanical properties also improved significantly: tensile strength and elongation increased by 9.5% and 45.7%, respectively, under 170 W ultrasonic treatment for 90 s.

Study [112] examined the effects of dissolved titanium, a chemical grain refiner (GR), and ultrasonic treatment (UT) on the solidification behaviour and microstructure of a 6xxx-series alloy (Al–1.0Mg–1.0Si) containing 1.0 wt.% Fe impurity. Primary aluminium grains and iron-containing intermetallic compounds (Fe IMCs, predominantly α-Al_8Fe_2Si/β-$Al_9Fe_2Si_2$) were identified *via* thermodynamic prediction and microscopy. The results demonstrated that ultrasonic treatment produced the finest and most homogeneous microstructure, improving both grain refinement and Fe IMC distribution, and outperforming chemical treatment methods.

During solidification, electromagnetic stirring alternating between clockwise and counter-clockwise directions was applied [113]. The resulting solidified structures were characterised relative to the timing of the stirring reversals. Compared to as-cast microstructures, those formed under electromagnetic stirring exhibited finer grains. The grain refinement mechanisms were shown to depend on the timing of the counter-clockwise stirring.

Ultrasonic surface treatment of laser-hardened AISI 1045 steel is recognised as an important technique to enhance surface properties such as roughness, waviness, grain size, phase composition, residual macrostress, and microhardness. Work [114] applied laser hardening (LHT) followed by ultrasonic impact treatment (UIT), also known as high-frequency mechanical impact treatment (HFMIT), to AISI 1045 steel. The subsurface microstructure after combined LHT + UIT was characterised using optical microscopy, transmission electron microscopy, and x-ray diffraction. Residual macrostresses, microhardness, roughness, and waviness were also measured. The results showed that LHT + UIT induced phase transformations and intense plastic deformation, producing layered hardened regions and refined grains in the subsurface of the medium-carbon steel.

Study [115] investigated the combined effect of bismuth modification and ultrasonic treatment on the microstructure and mechanical properties of AlMg5Si2Mn alloy. Compared to the untreated alloy, bismuth promoted MgSi formation through segregation and pre-solidification undercooling. Ultrasonic treatment enhanced the bismuth modification of the Mg_2Si eutectic phase and transformed the primary α-Al morphology in $AlMg_5Si_2Mn$ from coarse dendritic to fine, nearly spherical equiaxed grains, aiding melt homogenisation and uniform distribution of bismuth atoms or clusters.

Experiments [116–118] evaluated the combined influence of external and internal factors on the properties of complex-alloyed steels. It was determined that magnetic fields primarily influence hardness, while me-

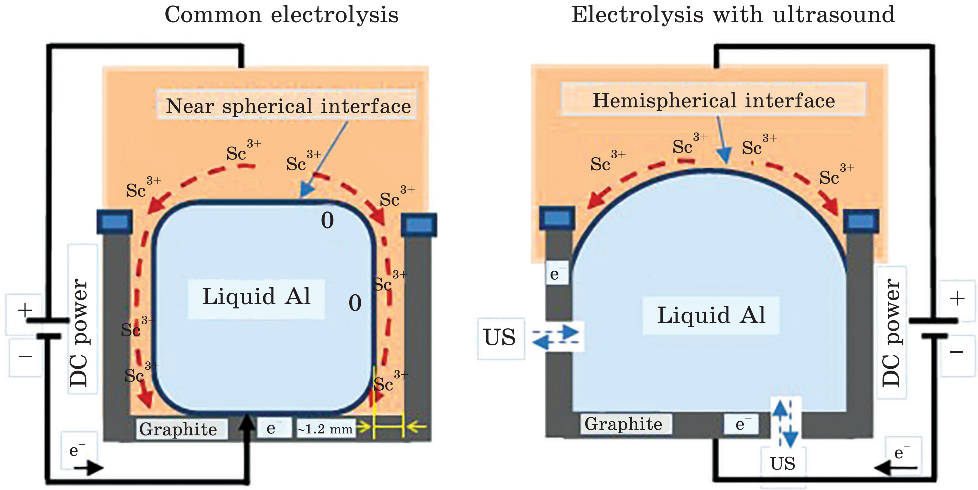

Fig. 7. Electrolytic Al–Sc system alloys and a schematic of the electrolysis process [119]

chanical oscillations enhance strength characteristics. It was suggested that oscillations exert a more pronounced effect on grain refinement throughout the entire ingot volume, whereas magnetic fields mainly affect the surface crystal layers in contact with the mould walls during solidification, promoting fragmentation and the creation of additional nucleation sites. An experimental matrix has been compiled.

In study [119], ultrasonic vibrations were applied during the formation of Al–Sc alloys using molten salt electrolysis. It was determined that ultrasound can significantly enhance the scandium content in the electrolytic Al–Sc alloy and refine Al_3Sc phase clusters into cubic-shaped particles.

Figure 7 presents photographs of the electrolytic Al–Sc alloys and a schematic illustration of the electrolysis process. The final Al–Sc alloy exhibits an almost spherical shape, as shown in Fig. 3, *a*. The diameter of the resulting alloy is approximately 17 mm, slightly smaller than the diameter of the cathodic chamber (20 mm). However, due to the poor wettability of liquid aluminium on graphite, the molten salt can penetrate the cathodic chamber. As a result, the interface assumes a nearly spherical shape, forming a channel (≈1.2 mm) that facilitates the transport of Sc_i^+ ions from the top to the bottom for the discharge reaction ($Sc_i^+ + 3e^- \rightarrow Sc$), as illustrated in Fig. 3, *b*.

As evident from the analysed sources, ultrasonic and electromagnetic treatment is employed to refine grains, improve homogeneity, and purify ingots in both ferrous and non-ferrous alloys. These treatments are also applicable in powder metallurgy, laser cladding, as well as in welding and brazing of metals and alloys. However, ultrasonic processing of liquid and solidifying metals has not yet gained wide industrial adoption due to several challenges associated with scaling up the process for large volumes of metal.

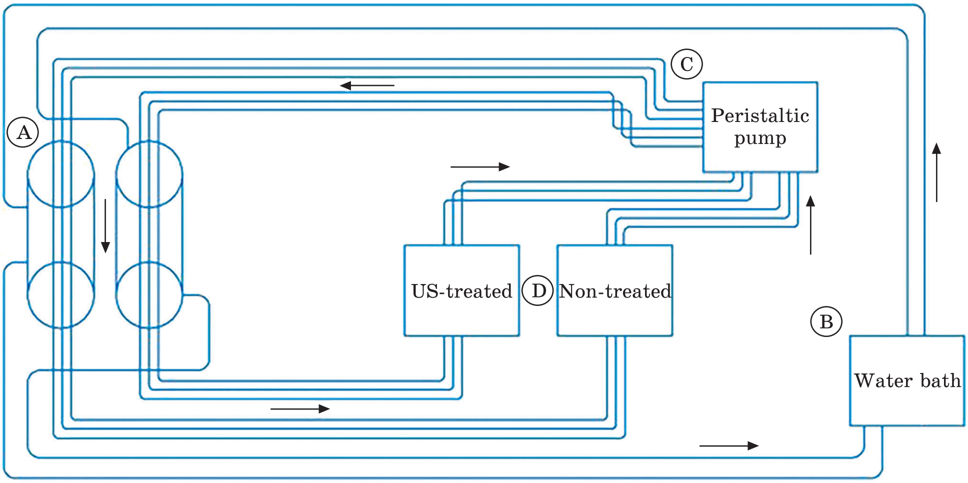

Fig. 8. Schematic diagram of the apparatus for dynamic immersion studies: *A* — acrylic columns with water at 37 °C, *B* — water bath, *C* — peristaltic pump, *D* — EBSS reservoir [121]

The microstructure and properties of 1030B aluminium strip were improved by applying UMT on the Hazelett continuous casting and direct rolling production line [120]. The microstructure and properties of the 1030B aluminium strip were examined using SEM, EBSD, and tensile testing. The application of UMT reduced the average grain size in the cast sheet by more than 28% compared to conventional samples without UMT.

The results reported in Ref. [121] showed that wire produced from ultrasonically treated ingots exhibited a faster initial corrosion rate than wire from untreated ingots during immersion in solution for up to 6 hours. This trend persisted with longer immersion times; however, the ultrasonically treated material demonstrated a lower overall corrosion rate and more uniform degradation, whereas the untreated material exhibited the localised corrosion features.

Figure 8 shows a schematic of the apparatus designed for performing dynamic immersion tests.

As evidenced by the reviewed literature, ultrasonic and electromagnetic treatments are widely employed to refine grains, enhance homogeneity, and clean ingots of both ferrous and non-ferrous alloys. These treatments are also applied in powder metallurgy, laser cladding, welding, and soldering of metals and alloys. However, ultrasonic processing of liquid and solidifying metals has yet to be widely industrialised, primarily due to the challenges of scaling up for large melt volumes.

Comprehensive melt processing using combined methods also shows promise for application in the production of complex-alloy steels.

5. Conclusions

External-field processing of metal melts (such as ultrasonic and electromagnetic treatment) is recognised as an effective method for improving the structure of solidified aluminium and magnesium alloys without altering their chemical composition. The literature provides an extensive array of melt-treatment techniques and solidification studies, offering valuable insights into the mechanisms of refinement and homogenisation.

It is particularly noteworthy that the synergistic application of internal and external treatments produces a homogeneous, defect-free ingot structure, thereby enabling a new level of material performance. Structural changes observed in the alloys include modified grain morphology, improved homogeneity, elimination of chemical segregation, reduction in non-metallic inclusions, and favourable conditions for the formation of high-dispersion reinforcing phases.

For alloyed steels, melt-treatment technology employing nanomodifiers and inoculants of diverse origin, followed by mechanical vibration and/or electromagnetic-field processing, is considered preferable. Nanoscale refractory carbide and oxide powders are suitable as nanomodifiers, while industrial casting and metallurgical waste serve as effective inoculants. Modifiers promote structural refinement by increasing the nucleation rate, whereas inoculants regulate the rate and uniformity of crystallisation.

The introduction of appropriate nanomodifiers enables the creation of materials of a 'new nature', namely, reinforced or composite ones, without significant alteration of the base chemical composition. In such materials, nanoparticles or newly introduced phases act as a structural 'framework' within the existing matrix. In this context, the concept of 'nanomodification' assumes a broader meaning, encompassing both structural refinement and the potential formation of new phases, *e.g.*, through the introduction of refractory-metal nanoparticles.

Acknowledgment. This research was carried out within the framework of the grant of the Science Committee of the Ministry of Science and Higher Education of the Republic of Kazakhstan (BR24993020), entitled 'Development and implementation of a technology for producing complex-alloyed steels with a homogeneous structure through the synergy of melt treatments'.

Authors' Contributions. A.Z.I. and V.Yu.K. devised the main conceptual ideas and supervised the project. A.Z.I. and S.V.K. reviewed the literature and collected the data on the mechanical properties. S.V.K. and V.Yu.K. developed the methodology and carried out the investigations. S.K.A. performed the formal analysis and provided the visualisation of the results. V.Yu.K. and S.V.K. wrote the original manuscript draft. A.A.T. translated the manuscript into English and performed the primary editing. The final version was further reviewed and refined by S.K.A. and A.A.T. All authors participated in writing the paper, approved the final version, and agreed to the published version of the manuscript.

REFERENCES

1. A. Hirata, T. Fujita, Y.R. Wen, J.H. Schneibel, C.T. Liu, and M.W. Chen, Atomic Structure of Nanoclusters in Oxide-Dispersion-Strengthened Steels, *Nat. Mater.*, **10**: 922 (2011);
https://doi.org/10.1038/nmat3115
2. M. Dade, J. Malaplate, J. Garnier, F. De Geuser, F. Barcelo, P. Wident, and A. Deschamps, Influence of Microstructural Parameters on the Mechanical Properties of Oxide Dispersion Strengthened Fe–14Cr Steels, *Acta Mater.*, **127**: 165 (2017);
https://doi.org/10.1016/j.actamat.2016.12.057
3. M. Kivio, L. Holappa, S. Louhenkilpi, M. Nakamoto, and T. Tanaka, Studies on Interfacial Phenomena in Titanium Carbide/Liquid Steel Systems for Development of Functionally Graded Material, *Metall. Mater. Trans. B*, **47**: 2114 (2016);
https://doi.org/10.1007/s11663-016-0640-y
4. J.J. Lewandowski and M. Seifi, Metal Additive Manufacturing: A Review of Mechanical Properties, *Annu. Rev. Mater. Res.*, **46**: 151 (2016);
https://doi.org/10.1146/annurev-matsci-070115-032024
5. T. DebRoy, H.L. Wei, J.S. Zuback, T. Mukherjee, J.W. Elmer, J.O. Milewski, A.M. Beese, A. Wilson-Heid, A. De, and W. Zhang, Additive Manufacturing of Metallic Components — Process, Structure and Properties, *Prog. Mater. Sci.*, **92**: 112 (2018);
https://doi.org/10.1016/j.pmatsci.2017.10.001
6. F. Lin, F. Jia, M. Ren, J. Wang, M. Yang, Z. Chen, and Z. Jiang, Microstructure, Mechanical and Thermal Properties of Ultrafine-Grained Al2024–TiC-GNPs Nanocomposite, *Mater. Sci. Eng. A*, **841**: 142855 (2022);
https://doi.org/10.1016/j.msea.2022.142855
7. W. Zhai, W. Zhou, and S.M.L. Nai, Effect of Interface Wettability on Additively Manufactured Metal Matrix Composites: A Case Study of 316L-Y_2O_3 Oxide Dispersion-Strengthened Steel, *Metals*, **14**: 170 (2024);
https://doi.org/10.3390/met14020170
8. H. Sakasegawa, S. Ohtsuka, S. Ukai, H. Tanigawa, M. Fujiwara, H. Ogiwara, and A. Kohyama, Microstructural Evolution during Creep of 9Cr-ODS Steels, *Fusion Eng. Des.*, **81**: 1013 (2006);
https://doi.org/10.1016/j.fusengdes.2005.08.048
9. Y. Zhong, L. Liu, J. Zou, X. Li, D. Cui, and Z. Shen, Oxide Dispersion Strengthened Stainless Steel 316L with Superior Strength and Ductility by Selective Laser Melting, *J. Mater. Sci. Technol.*, **42**: 97 (2020);
https://doi.org/10.1016/j.jmst.2019.10.003
10. J.R.O. Leo, S.P. Barroso, M.E. Fitzpatrick, M. Wang, and Z. Zhou, Microstructure, Tensile and Creep Properties of an Austenitic ODS 316L Steel, *Mater. Sci. Eng. A*, **749**: 158 (2019);
https://doi.org/10.1016/j.msea.2019.01.110
11. A. Durga, N.H. Pettersson, S.B.A. Malladi, Z. Chen, S. Guo, L. Nyborg, and G. Lindwall, Grain Refinement in Additively Manufactured Ferritic Stainless Steel by *in situ* Inoculation Using Pre-Alloyed Powder, *Scr. Mater.*, **194**: 113690 (2021);
https://doi.org/10.1016/j.scriptamat.2020.113690
12. V. Dyakova, Ya. Kostova, V. Manolov, P. Kuzmanov, Iv. Panov, A. Velikov, and B. Dochev, Comparative Study of the Influence of Some Nanomodifiers on the Mi-

crostructure and Corrosion Properties of AlSi18 Alloy, *J. Chem. Technol. Metall.*, **56**, No. 1: 205 (2021).
13. P.V. Kovalev, A.Z. Isagulov, S.D. Popova, V.Yu. Kulikov, and St.S. Kvon, Investigation of the Effect of High Strength Strips Steel Modification with Rare-Earth Metal, *Metalurgija*, **56**, Nos. 3–4: 393 (2017).
14. P.V. Kovalev, A.Z. Isagulov, S.D. Popova, V.Yu. Kulikov, and St.S. Kvon, Improving Shipbuilding Steel Grade Quality at Stages of Smelting, Secondary Refining, and Continuous Casting, *Metals*, **9**, No. 2: 203 (2019); https://doi.org/10.3390/met9020203
15. A.Z. Issagulov, Sv.S. Kvon, Ye.V. Svortsov, and V.Yu. Kulikov, Nanomodifier Effect on Structure and Properties Changes of Heat-Treatable Steel, *Metalurgija*, **59**, No. 4: 540 (2020).
16. Q. Gu, X. Huang, J. Xi, and Z. Gao, The Influence of Magnetic Field on Fatigue and Mechanical Properties of a 35CrMo Steel, *Metals*, **11**: 542 (2021); https://doi.org/10.3390/met11040542
17. K.N. Vdovin, G.A. Dubskiy, and L.G. Egorova, Vliyanie Magnitnogo Polya na Protsess Kristallizatsii Alyuminievykh Rasplavov [Influence of Magnetic Field on the Crystallisation Process of Aluminium Melts], *Izvestiya Vuzov. Tsvetnaya Metallurgiya*, No. 2: 34 (2018) (in Russian); https://doi.org/10.17073/0021-3438-2018-2-34-42
18. A. Freitas, F. Landgraf, M.M. Seckler, and M. Giulietti, The Influence of Magnetic Field on Crystallisation from Solutions, *Proc. Int. Conf. Ind. Crystall. (September 1999, Cambridge, UK)*, p. 215.
19. Y.Q. Wang, M. Gorley, S. Kabra, and E. Surrey, Influence of a 1.5 T Magnetic Field on the Tensile Properties of Eurofer-97 Steel, *Fusion Eng. Des.*, **141**: 68 (2019); https://doi.org/10.1016/j.fusengdes.2019.03.017
20. V. Braic, A. Vladescu, M. Balaceanu, C.R. Luculescu, and M. Braic, Nanostructured multi-element (TiZrNbHfTa)C hard coatings, *Surf. Coat. Technol.*, **211**: 117 (2012); https://doi.org/10.1016/j.surfcoat.2011.09.033
21. Z. Liu, S. Zhang, F. Cao, S. Liang, and T. Wang, Effect of Ultrasonic Vibration Treatment on Microstructure Evolution and Mechanical Properties of Cu-TiB~2~ Composites, *Mater. Charact.*, **211**: 113912 (2024); https://doi.org/10.1016/j.matchar.2024.113912
22. K.G. Basavakumar, P.G. Mukunda, and M. Chakraborty, Influence of Grain Refinement and Modification on Microstructure and Mechanical Properties of Al–7Si and Al–7Si–2.5Cu Cast Alloys, *Mater. Charact.*, **59**: 283 (2008); https://doi.org/10.1016/j.matchar.2007.01.011
23. T. Pan, Y. Zhi, W. Zou, J. Nie, Y. Fan, R. Liu, H. Chen, G. Zhong, Y. Zhou, C. Li, and X. Liu, Achieving Significant Grain Refinement and Enhanced Mechanical Properties of Sand-Cast ZL114A Alloy by a New Synergetic Addition Strategy of Al-TCB Grain Refiner and Sr Modifier, *J. Alloys Compd.*, **1018**: 179246 (2025); https://doi.org/10.1016/j.jallcom.2025.179246
24. K. Suo, Y. Xu, W. Ma, Y. Ren, and Y. Lei, Separation of Al–Si–(Fe, Ni) Melt for Simultaneous Recycling of Al–Si Scrap and Preparation of Al–Si Eutectic Alloys, *Sep. Purif. Technol.*, **363**, Pt. 1: 132032 (2025); https://doi.org/10.1016/j.seppur.2025.132032
25. J. Dong, J. Jiang, Y. Wang, M. Huang, J. Cui, T. Qin, and L. Kong, Effect of Er, Zr, V, Ti Microalloying and Multi-Field Coupling Melt Deep Purification on the Microstructure and Mechanical Properties of Al–12Si–4.5Cu–2Ni Alloy, *Mater. Sci. Eng. A*, **923**: 147706 (2025);

https://doi.org/10.1016/j.msea.2024.147706

26. I. Spacil, A. Hohenwarter, P. Hofer-Hauser, and J. Li, Linking Microstructure with Static and Dynamic Mechanical Properties of Al–7Si–0.3Mg Based Alloys, *J. Alloys Compd.*, **1032**: 181161 (2025); https://doi.org/10.1016/j.jallcom.2025.181161
27. G.E. Akhmetova, G.A. Ulyeva, and K.N. Tuyskhan, On the Issue of Alloying and Modification of Alloys: Using the Waste Products for Creation of Novel Materials, *Prog. Phys. Met.*, **22**, No. 2: 271 (2021); https://doi.org/10.15407/ufm.22.02.271
28. D. Yang, C. Yuehua, D. Song, D. Yang, Y. Zhao, W. Xiangjie, N. Zhou, Z.-Q. Guo, and B. Ke, A Novel Modifier Al–Sr–RE for Improving the Microstructure and Mechanical Properties of Recycled AA3104 Alloy, *J. Alloys Compd.*, **1022**: 179744 (2025); https://doi.org/10.1016/j.jallcom.2025.179744
29. B. Dochev, V. Manolov, A. Velikov, V. Diyakova, and P. Kuzmanov, Investigation of the Potential of Simultaneous Modification of Hypereutectic Aluminum-Silicon AlSi18 Alloy with Conventional and Nano-Modifier, *IFAC-PapersOnLine*, **52**, No. 25: 488 (2019); https://doi.org/10.1016/j.ifacol.2019.12.590
30. J.-Y. Lee, J.-M. Lee, K.-S. Son, J.-I. Jang, and Y.-H. Cho, A Study on the Interaction between a Sr Modifier and an Al-5Ti-1B Grain Refiner in an Al-7Si-0.35Mg Casting Alloy, *J. Alloys Compd.*, **938**: 168598 (2023); https://doi.org/10.1016/j.jallcom.2022.168598
31. A.M. Samuel, G.H. Garza-Elizondo, H.W. Doty, and F.H. Samuel, Role of Modification and Melt Thermal Treatment Processes on the Microstructure and Tensile Properties of Al–Si Alloys, *Mater. Des.*, **80**: 99 (2015); https://doi.org/10.1016/j.matdes.2015.05.013
32. P. Yan, W. Mao, J. Fan, B. Wang, and Y. Liu, Microstructural Evolution, Segregation and Fracture Behavior of A390 Alloy Prepared by Combined Rheo-HPDC Processing and Sr-Modifier, *J. Alloys Compd.*, **835**: 155297 (2020); https://doi.org/10.1016/j.jallcom.2020.155297
33. M.F. Kilicaslan and E. Karakцse, Production of CNT-Bearing Melt-Spun Al-2Sc-0.05CNT Alloys, *J. Alloys Compd.*, **738**: 182 (2018); https://doi.org/10.1016/j.jallcom.2017.12.130
34. Q. Luo, X. Li, Q. Li, L. Yuan, L. Peng, F. Pan, and W. Ding, Achieving Grain Refinement of α-Al and Si Modification Simultaneously by La-B-Sr Addition in Al-10Si Alloys, *J. Mater. Sci. Technol.*, **135**: 97 (2023); https://doi.org/10.1016/j.jmst.2022.07.009
35. P. Tang, Q. Liu, F. Yu, F. Mo, and L. Qin, Effect and Its Mechanism of Fixed-Ratio and Incremented 3Be–Sb Complex Modifier on Microstructures and Properties of Hypereutectic Al–Si–Mg Alloy, *J. Alloys Compd.*, **931**: 167478 (2023); https://doi.org/10.1016/j.jallcom.2022.167478
36. T. Jiang, C. Yu, B. Xu, W. Yu, G. Xu, Y. Li, Z. Wang, and G. Wang, A Novel Investigation on the Influence of Cu–P Modifier on the Microstructure, Mechanical Performance, and Melting Process of Al–50Si Alloys Treated by Overheating, *Prog. Nat. Sci. Mater. Int.*, **31**: 461 (2021); https://doi.org/10.1016/j.pnsc.2021.04.003
37. S.O. Polishko, Influence of Modification on the Characteristics of Reinforcing Steels Intended for Reinforced Concrete Structures, *Prog. Phys. Met.*, **24**, No. 3: 470 (2023); https://doi.org/10.15407/ufm.24.03.470

38. N.K. Kund, Influence of Melt Pouring Temperature and Plate Inclination on Solidification and Microstructure of A356 Aluminum Alloy Produced Using Oblique Plate, *Trans. Nonferrous Met. Soc. China*, **24**: 3465 (2014); https://doi.org/10.1016/S1003-6326(14)63490-7
39. E.B. Moustafa, H.D. Natto, E.M. Banoqitah, M.A. Alazwari, A.O. Mosleh, and A.M. Khalil, Improving the Mechanical and Dynamic Properties of Al–Zn–Mg–Cu–Based Aluminum Alloy: A Combined Approach of Microstructural Modification and Heat Treatment, *J. Alloys Compd.*, **1013**: 178558 (2025); https://doi.org/10.1016/j.jallcom.2025.178558
40. C. Li, Z. Wang, Y. Zhao, J. Du, Y. Ma, J. Li, and F. Sun, Modification Mechanism of Te and Morphology Evolution of Primary Mg_2Si in an Al–20Mg_2Si Alloy, *Heliyon*, **10**: e40141 (2024); https://doi.org/10.1016/j.heliyon.2024.e40141
41. M. Alipour, B.G. Aghdam, H.E. Rahnoma, and M. Emamy, Investigation of the Effect of Al–5Ti–1B Grain Refiner on Dry Sliding Wear Behavior of an Al–Zn–Mg–Cu Alloy Formed by Strain-Induced Melt Activation Process, *Mater. Des.*, **46**: 766 (2013); https://doi.org/10.1016/j.matdes.2012.10.058
42. G.-L. Liu, N.-C. Si, S.-C. Sun, and Q.-F. Wu, Effects of Grain Refining and Modification on Mechanical Properties and Microstructures of Al–7.5Si–4Cu Cast Alloy, *Trans. Nonferrous Met. Soc. China*, **24**: 946 (2014); https://doi.org/10.1016/S1003-6326(14)63147-2
43. J. Ding, C. Lu, Y. Sun, C. Cui, and E. Zhao, Refining and Modification Effects of (Al, Zr, Si)-Al~4~Sr on Al–7Si–0.5 Mg Alloy, *J. Mater. Res. Technol.*, **15**: 1604 (2021); https://doi.org/10.1016/j.jmrt.2021.09.006
44. M. Zuo, D. Zhao, X. Teng, H. Geng, and Z. Zhang, Effect of P and Sr Complex Modification on Si Phase in Hypereutectic Al–30Si Alloys, *Mater. Des.*, **47**: 857 (2013); https://doi.org/10.1016/j.matdes.2012.12.054
45. S. Wang, F. Kimura, W. Chen, J. Sang, H. Hirahara, and Y. Kajihara, Submicrometer Analyses of the Polymer Flow Modifier Effects on Metal-Polymer Direct Joining, *Mater. Lett.*, **347**: 134655 (2023); https://doi.org/10.1016/j.matlet.2023.134655
46. D.-Y. Wu, J. Kang, Z.-H. Feng, R. Su, C.-H. Liu, T. Li, and L.-S. Wang, Utilizing a Novel Modifier to Realize Multi-Refinement and Optimized Heat Treatment of A356 Alloy, *J. Alloys Compd.*, **791**: 628 (2019); https://doi.org/10.1016/j.jallcom.2019.03.327
47. H. Xi, W. Xiao, H. Li, Y. Fu, G. Yi, J. Qie, X. Ma, and C. Ma, Effects of Submicron-Sized TiC Particles on the Microstructure Modification and Mechanical Properties of Al–Si–Mg Alloy, *J. Alloys Compd.*, **968**: 171963 (2023); https://doi.org/10.1016/j.jallcom.2023.171963
48. A. Sarkar, S. Manivannan, and S.P.K. Babu, Modification of Al-11.1Si Alloy with Sodium through Casting Route, *Mater. Today Proc.*, **44**: 2781 (2021); https://doi.org/10.1016/j.matpr.2020.12.757
49. Y.-L. Zhou, W.-H. Song, Y.-X. Lai, and J.-H. Chen, Microstructural Role of TiB Addition in Modifying ZnAl Alloy, *Trans. Nonferrous Met. Soc. China*, **33**: 2726 (2023); https://doi.org/10.1016/S1003-6326(23)66293-4
50. Y.K. Singla, M.R. Maughan, N. Arora, and D.K. Dwivedi, Enhancing the Wear Resistance of Iron-Based Alloys: A Comprehensive Review of Alloying Element Ef-

fects, *J. Manuf. Process.*, **120**: 135 (2024);
https://doi.org/10.1016/j.jmapro.2024.04.038
51. A.S. Kandemir and R. Gecu, Influence of Vanadium Content and Cooling Rate on the Characteristics of Vanadium-Alloyed Spheroidal Graphite Cast Irons, *J. Alloys Compd.*, **934**: 168017 (2023);
https://doi.org/10.1016/j.jallcom.2022.168017
52. A. Vasko, Comparison of Mechanical and Fatigue Properties of SiMo- and SiCu-Types of Nodular Cast Iron, *Mater. Today Proc.*, **32**: 168 (2020);
https://doi.org/10.1016/j.matpr.2020.04.184
53. X. Yao, T. Jiang, S. Wei, L. Xu, K. Pan, H. Yu, C. Chen, C. Zhang, X. Wang, and C. Wang, Microstructure and Abrasive Wear Performance of a Novel CALPHAD-Inspired Wear-Resistant Steel Containing Multiphase and Multiscale Carbides, *Wear*, **538–539**: 205182 (2024);
https://doi.org/10.1016/j.wear.2023.205182
54. F. Qiu, H. Zhang, C.-L. Li, Z.-F. Wang, F. Chang, H.-Y. Yang, C.-D. Li, X. Han, and Q.-C. Jiang, Simultaneously Enhanced Strength and Toughness of Cast Medium Carbon Steels Matrix Composites by Trace Nano-Sized TiC Particles, *Mater. Sci. Eng. A*, **819**: 141485 (2021);
https://doi.org/10.1016/j.msea.2021.141485
55. N. Li, F. Ge, S. Wu, H. Tan, and Z. Hu, *J. Alloys Compd.*, **1024**: 180249 (2025);
https://doi.org/10.1016/j.jallcom.2025.180249
56. H. Xie, L. Xu, X. Deng, X. Diao, Z. Li, and S. Wei, Effect of Silicon on Microstructure and Wear Properties of Bainite High Vanadium Wear-Resistant Alloy, *Wear*, 205784 (2025);
https://doi.org/10.1016/j.wear.2025.205784
57. M.P. Moodispaw, J. Miao, E. Cinkilic, and A.A. Luo, The Beneficial Effect of Ce Additions to High Fe-Containing Secondary Al–Si–Mg Cast Alloys, *J. Alloys Compd.*, **1009**: 176864 (2024);
https://doi.org/10.1016/j.jallcom.2024.176864
58. X. Wang, Z. Wu, B. Li, W. Chen, J. Zhang, and J. Mao, Inclusions Modification by Rare Earth in Steel and the Resulting Properties: A Review, *J. Rare Earths*, **42**: 431 (2024);
https://doi.org/10.1016/j.jre.2023.04.015
59. W. Liu, J. Wang, M. Sun, B. Xu, J. Yao, Q. Fan, and D. Li, Cerium Refinement of Grains and Primary Carbides during Solidification of Cr4Mo4V Bearing Steel, *J. Rare Earths*, **42**: 783 (2024);
https://doi.org/10.1016/j.jre.2023.05.001
60. S.K. Arinova, D.R. Aubakirov, M.M. Dospayev, A.A. Tuganbayeva, *Acta Metall. Slovaca*, **31**, No. 2: 108 (2025);
https://doi.org/10.36547/ams.31.2.2212
61. A.Z. Issagulov, O.A. Sharaya, N.V. Vodolazskaya, S.K. Arinova, A.A. Tugambaeva, *Mater. Mech. Eng. Technol.*, No. 2: 38 (2025) (in Russian).
https://doi.org/10.52209/2706-977X_2025_2_38
62. M. Sun, X. Nie, Z. Chen, L. Liang, L. Guo, M. Wang, C. Zhao, and L. Li, Improved Low-Stress Thermoplastic Forming of TiAl Alloys *via* Dislocation Behavior under Mechanical Vibration, *J. Alloys Compd.*, **1022**: 180030 (2025);
https://doi.org/10.1016/j.jallcom.2025.180030
63. Z. Zuo, M. Paidar, R.V. Vignesh, H. Keshavrazi, S. Alamri, and X. Liu, Evaluating the Influence of Vibrational Assistance Friction Stir Processing on Improving the Wear and Mechanical Properties of Hybrid Composite AZ31 Mg Alloy, *J. Mater. Res. Technol.*, **36**: 5040 (2025);

https://doi.org/10.1016/j.jmrt.2025.04.180
64. B. Lin, X.-X. He, S.-C. Xia, H.-Q. Xiao, Y.-L. Zhao, and K. Khanlari, Effect of Ultrasonic and Mechanical Vibration Treatments on Evolution of Mn-Rich Phases and Mechanical Properties of Al–12Si–4Cu–1Ni–1Mg–2Mn Piston Alloys, *Trans. Nonferrous Met. Soc. China*, **34**: 2393 (2024); https://doi.org/10.1016/S1003-6326(24)66549-0
65. C. Guo, T. Qu, Y. Yu, and J. Zhou, Interaction Impact of Mechanical Vibration and Fin Structure on the Melting Heat Transfer Characteristics of Phase Change Materials, *J. Energy Storage*, **114**, Pt. B: 115927 (2025); https://doi.org/10.1016/j.est.2025.115927
66. S.N. Lan, Y. Shi, J.Q. Yao, L.J. Xie, S.M. Yin, K. Wang, and X.W. Liu, Refined Microstructure to Improve the Mechanical Properties of the As-Cast NiCoCr Multi Principal Element Alloy *via* Mechanical Vibration, *Mater. Lett.*, **365**: 136409 (2024); https://doi.org/10.1016/j.matlet.2024.136409
67. Saifudin, N. Muhayat, E. Surojo, M.R. Muslih, and Triyono, Effect of Vibration Frequency on Mechanical Properties and Microstructure of Metal Inert Gas Welded Dissimilar AA5083 and AA6061 Aluminum Alloy Joints, *Results Eng.*, **24**: 102970 (2024); https://doi.org/10.1016/j.rineng.2024.102970
68. Y. Liu, X. Li, R. Guo, Z. Li, J. Du, M. Liu, Q. Hu, X. Kong, and L. Bao, Effect of Mechanical Vibration on Microstructure and Impact Properties of Gas Metal Arc Welding Q450NQR1 Welded Joints, *Int. J. Press. Vessel. Pip.*, **213**: 105371 (2025); https://doi.org/10.1016/j.ijpvp.2024.105371
69. V.-T. Pham, T.-N. Vu, T.-H. Fang, D.-B. Luu, V.-T. Hoang, N.-H. Tran, M.-S. Tran, and Q.-B. Tao, Effects of Microstructure and Vibration Parameters on Mechanical Properties of Nanoimprinted FeNiCrCoCu High-Entropy Alloys, *Physica B*, **665**: 415028 (2023); https://doi.org/10.1016/j.physb.2023.415028
70. H.-M. Guo, A.-S. Zhang, X.-J. Yang, and M.-M. Yan, Grain Refinement of Al-5%Cu Aluminum Alloy under Mechanical Vibration Using Meltable Vibrating Probe, *Trans. Nonferrous Met. Soc. China*, **24**: 2489 (2014); https://doi.org/10.1016/S1003-6326(14)63375-6
71. X. Shao, Y. Chenxu, B. Wang, N. Zhang, and Y. Yuan, Mechanical Agitation Triggered Crystallization of Eutectic Phase Change Material Xylitol/Erythritol with Persistent Supercooling for Controllable Heat Retrieval, *Sol. Energy Mater. Sol. Cells*, **256**: 112335 (2023); https://doi.org/10.1016/j.solmat.2023.112335
72. L. Zhang, W. Bian, K. Fu, X. Dai, H. Wang, and J. Wang, Improvement of Mechanical Properties and Microstructure of Wire Arc Additive Manufactured 2319 Aluminum Alloy by Mechanical Vibration Acceleration, *Mater. Charact.*, **208**: 113672 (2024); https://doi.org/10.1016/j.matchar.2024.113672
73. C. Jinxia, C. Xu, and Z. Luo, Effect of Mechanical Vibration on Microstructure and Properties of Cast AZ91D Alloy, *Results Phys.*, **11**: 1022 (2018); https://doi.org/10.1016/j.rinp.2018.10.047
74. T.K. Chavan, Influence of Mould Vibration on Microstructural Behaviour and Mechanical Properties of LM25 Aluminium Alloy Using Gravity Die Casting Process, *Mater. Today Proc.*, **46**: 4412 (2021); https://doi.org/10.1016/j.matpr.2020.09.671
75. W. Jiang, Z. Fan, X. Chen, B. Wang, and H. Wu, Combined Effects of Mechanical Vibration and Wall Thickness on Microstructure and Mechanical Properties of A356 Aluminum Alloy Produced by Expendable Pattern Shell Casting, *Mater. Sci.*

Eng. A, **619**: 228 (2014);
https://doi.org/10.1016/j.msea.2014.09.102
76. F. Taghavi, H. Saghafian, and Y.H.K. Kharrazi, Study on the Effect of Prolonged Mechanical Vibration on the Grain Refinement and Density of A356 Aluminum Alloy, *Mater. Des.*, **30**: 1604 (2009);
https://doi.org/10.1016/j.matdes.2008.07.032
77. A.K. Ghosh and P. Halder, Mechanical Vibration Effects on the Melting Performance of Nano-Enhanced Phase Change Material, *Appl. Therm. Eng.*, **269**, Pt. A: 125986 (2025);
https://doi.org/10.1016/j.applthermaleng.2025.125986
78. C. Limmaneevichitr, S. Pongananpanya, and J. Kajornchaiyakul, Metallurgical Structure of A356 Aluminum Alloy Solidified under Mechanical Vibration: An Investigation of Alternative Semi-Solid Casting Routes, *Mater. Des.*, **30**: 3925 (2009);
https://doi.org/10.1016/j.matdes.2009.01.036
79. R.-J. Wang, S.-P. Wu, and W. Chen, Mechanism of Burst Feeding in ZL205A Casting under Mechanical Vibration and Low Pressure, *Trans. Nonferrous Met. Soc. China*, **28**: 1514 (2018);
https://doi.org/10.1016/S1003-6326(18)64792-2
80. K. Kocatepe, Effect of Low Frequency Vibration on Porosity of LM25 and LM6 Alloys, *Mater. Des.*, **28**: 1767 (2007);
https://doi.org/10.1016/j.matdes.2006.05.004
81. S. Pan, Y. Liu, B. Yang, Y. Fu, M. Gao, and R. Guan, Effect of Stirring Speed and Temperature on the Microstructure and Mechanical Properties of A356 Alloy under Vacuum, *Vacuum*, **212**: 112059 (2023);
https://doi.org/10.1016/j.vacuum.2023.112059
82. L. Xie, H. Sun, Y. Wen, L. Hua, and L.-C. Zhang, Electromagnetic Treatment Enhancing Performance of Metal Materials: A Review, *Prog. Mater. Sci.*, **153**: 101488 (2025);
https://doi.org/10.1016/j.pmatsci.2025.101488
83. M. Li, T. Tamura, and K. Miwa, Controlling Microstructures of AZ31 Magnesium Alloys by an Electromagnetic Vibration Technique during Solidification: From Experimental Observation to Theoretical Understanding, *Acta Mater.*, **55**: 4635 (2007);
https://doi.org/10.1016/j.actamat.2007.04.035
84. C.-K. Liu and Z.-Z. He, Compact Integrated Electromagnetic Driving of Liquid Metal for High Heat-Flux Dissipation, *Int. J. Therm. Sci.*, **211**: 109725 (2025);
https://doi.org/10.1016/j.ijthermalsci.2025.109725
85. M.H. Avnaim, B. Mikhailovich, A. Azulay, and A. Levy, Numerical and Experimental Study of the Traveling Magnetic Field Effect on the Horizontal Solidification in a Rectangular Cavity Pt. 1: Liquid Metal Flow under the TMF Impact, *Int. J. Heat Fluid Flow*, **69**: 23 (2018);
https://doi.org/10.1016/j.ijheatfluidflow.2017.11.003
86. A.D. Pogrebnyak, E.A. Bazyl, and N.V. Sviridenko, The Effect of Irradiation with Electron and Ion Beams on the Physical and Mechanical Properties of Titanium Alloys, *Prog. Phys. Met.*, **5**, No. 2: 257 (2004);
https://doi.org/10.15407/ufm.05.02.257
87. Y. Jia, X. Chen, Q. Le, and Y. Xin, The Role of Different Electromagnetic Fields in Magnesium Alloys Direct-Chill Casting: Numerical Simulation and Experimental Investigation, *J. Magnes. Alloys*, **12**: 5005 (2024);
https://doi.org/10.1016/j.jma.2024.01.036
88. J. Wang, Y. Zuo, Q. Zhu, R. Wang, X. Guo, and X. Liu, Simulation Study on the

Influence of the Combined Application of Melt Shearing and Electromagnetic Field on the Flow and Temperature Fields during Direct-Chill Casting of 2024 Aluminum Alloy, *Int. J. Heat Fluid Flow*, **113**: 109782 (2025);
https://doi.org/10.1016/j.ijheatfluidflow.2025.109782
89. A.B. Naizabekov, A.S. Kolesnikov, M.A. Latypova, T.D. Fedorova, and A.D. Mamitova, Current Trends to Obtain Metals and Alloys with Ultrafine-Grained Structure, *Prog. Phys. Met.*, **23**, No. 4: 629 (2022);
https://doi.org/10.15407/ufm.23.04.629
90. Y. Huang, J. Wen, Y. Liu, and Y. Zhao, Effects of Electromagnetic Frequency on the Microstructure and Mechanical Properties of $Al_{70}Zn_{10}Mg_{10}Cu_5Si_5$, *J. Mater. Res. Technol.*, **17**: 3105 (2022);
https://doi.org/10.1016/j.jmrt.2022.02.034
91. T. Tamura, M. Li, K. Takahashi, and E. Inoue, Improved Solidification Structures and Mechanical Properties of Al-20 wt% Sn Alloys Processed by an Electromagnetic Vibration Technique, *Mater. Sci. Eng. A*, **862**: 144416 (2023);
https://doi.org/10.1016/j.msea.2022.144416
92. V.O. Abramov, A.V. Abramova, V.M. Bayazitov, R.V. Nikonov, and G. Cravotto, Pores-Free Aluminium Alloy by Efficient Degassing Ultrasonic Treatments, *Appl. Acoust.*, **184**: 108343 (2021);
https://doi.org/10.1016/j.apacoust.2021.108343
93. M. Li, N. Omura, Y. Murakami, I. Matsui, and S. Tada, A Comparative Study of the Primary Phase Formation in Al–7 wt% Si and Al–17 wt% Si Alloys Solidified by Electromagnetic Stirring Processing, *Mater. Today Commun.*, **24**: 101146 (2020);
https://doi.org/10.1016/j.mtcomm.2020.101146
94. Z. Jiang, L. Zhu, J. Zhang, G. Meng, Z. Yang, and L. Xu, Influence of Ultrasonic Vibration on Molten Pool Behavior, Cladding Layer Microstructure and Pore Defects for Directed Energy Deposition, *Appl. Therm. Eng.*, **247**: 123047 (2024);
https://doi.org/10.1016/j.applthermaleng.2024.123047
95. C. He, Y. Li, J. Li, G. Xu, Z. Wang, and D. Wu, Effect of Electromagnetic Fields on Microstructure and Mechanical Properties of Sub-Rapid Solidification-Processed Al–Mg–Si Alloy during Twin-Roll Casting, *Mater. Sci. Eng. A*, **766**: 138328 (2019);
https://doi.org/10.1016/j.msea.2019.138328
96. M.K. Aghayani and B. Niroumand, Effects of Ultrasonic Treatment on Microstructure and Tensile Strength of AZ91 Magnesium Alloy, *J. Alloys Compd.*, **509**: 114 (2011);
https://doi.org/10.1016/j.jallcom.2010.08.139
97. B. Nagasivamuni, G. Wang, D.H. StJohn, and M.S. Dargusch, The Effect of Ultrasonic Treatment on the Mechanisms of Grain Formation in As-Cast High Purity Zinc, *J. Cryst. Growth*, **495**: 20 (2018);
https://doi.org/10.1016/j.jcrysgro.2018.05.006
98. S. Guo, Q. Le, Z. Zhao, Z. Wang, and J. Cui, Microstructural Refinement of DC Cast AZ80 Mg Billets by Low Frequency Electromagnetic Vibration, *Mater. Sci. Eng. A*, **404**: 323 (2005);
https://doi.org/10.1016/j.msea.2005.05.070
99. T. Tamura and M. Li, Separation of Aluminum and Silicon from Crystallizing Al–12.6 wt%Si Eutectic Melts by Applying an Electromagnetic Force during Directional Solidification, *J. Mater. Process. Technol.*, **342**: 118916 (2025);
https://doi.org/10.1016/j.jmatprotec.2025.118916
100. N. Balasubramani, J. Venezuela, D. StJohn, G. Wang, and M. Dargusch, A Review of the Origin of Equiaxed Grains during Solidification under Mechanical

Stirring, Vibration, Electromagnetic, Electric-Current, and Ultrasonic Treatments, *J. Mater. Sci. Technol.*, **144**: 243 (2023);
https://doi.org/10.1016/j.jmst.2022.09.067
101. G. Tang, Z. Sun, B. Luo, W. Lin, Z. Lin, T. Zheng, B. Zhou, P. Shi, Q. Li, C. Liu, H. Lu, Z. Shen, B. Ding, and Y. Zhong, Study on the Structural Evolution of Al–15Sn–1Cu Alloys Solidified at Different Electromagnetic Vibration Frequencies, *J. Mater. Process. Technol.*, **338**: 118771 (2025);
https://doi.org/10.1016/j.jmatprotec.2025.118771
102. Z. Liu, S. Zhang, F. Cao, Y. Jiang, Z. Chen, H. Kang, Z. Cao, E. Guo, S. Liang, and T. Wang, Effect of Ultrasonic Vibration Treatment on Microstructure Evolution and Mechanical Properties of $Cu–TiB_2$, *Mater. Charact.*, **211**: 113912 (2024);
https://doi.org/10.1016/j.matchar.2024.113912
103. G. Tang, Z. Sun, Z. Lin, T. Zheng, B. Zhou, P. Shi, Q. Li, C. Liu, H. Lu, Z. Shen, B. Ding, and Y. Zhong, Revealing the Influential Mechanism of Electromagnetic Vibration on the Bulk Solidification and the Upward Continuous Casting of Cu–15Ni–8Sn Alloy, *J. Mater. Sci. Technol.*, **189**: 166 (2024);
https://doi.org/10.1016/j.jmst.2023.12.019
104. Q. Li, W. Jiang, Y. Xu, L. Yu, Z. Peng, Y. Xin, and Z. Fan, Influence of Gd Alloying and Ultrasonic Vibration Hybrid Treatment on the Microstructures, Mechanical Properties and Strengthening Mechanisms of Al/Mg Interface by Compound Casting, *J. Mater. Res. Technol.*, **35**: 1040 (2025);
https://doi.org/10.1016/j.jmrt.2025.01.083
105. T. Nagira, N. Nakatsuka, H. Yasuda, K. Uesugi, A. Takeuchi, and Y. Suzuki, Impact of Melt Convection Induced by Ultrasonic Wave on Dendrite Growth in Sn–Bi Alloys, *Mater. Lett.*, **150**: 135 (2015);
https://doi.org/10.1016/j.matlet.2015.02.069
106. X. Chen, Y. Jia, Q. Liao, W. Jia, Q. Le, S. Ning, and F. Yu, The Simultaneous Application of Variable Frequency Ultrasonic and Low Frequency Electromagnetic Fields in Semi Continuous Casting of AZ80 Magnesium Alloy, *J. Alloys Compd.*, **774**: 710 (2019);
https://doi.org/10.1016/j.jallcom.2018.09.300
107. J.-Z. Cui, Z.-Q. Zhang, and Q.-C. Le, Direct-Chilling Casting of Mg Alloy under Electromagnetic and Ultrasonic Combined Field, *Trans. Nonferrous Met. Soc. China*, **20**: s297 (2010);
https://doi.org/10.1016/S1003-6326(10)60487-6
108. F. Wang, D. Eskin, J. Mi, C. Wang, B. Koe, A. King, C. Reinhard, and T. Connolley, A Synchrotron X-Radiography Study of the Fragmentation and Refinement of Primary Intermetallic Particles in an Al–35Cu Alloy Induced by Ultrasonic Melt Processing, *Acta Mater.*, **141**: 142 (2017);
https://doi.org/10.1016/j.actamat.2017.09.010
109. J. Barbosa and H. Puga, Ultrasonic Melt Processing in the Low Pressure Investment Casting of Al Alloys, *J. Mater. Process. Technol.*, **244**: 150 (2017);
https://doi.org/10.1016/j.jmatprotec.2017.01.031
110. Z.-W. Shao, Q.-C. Le, J.-Z. Cui, and Z.-Q. Zhang, Numerical Simulation of Standing Waves for Ultrasonic Purification of Magnesium Alloy Melt, *Trans. Nonferrous Met. Soc. China*, **20**: s382 (2010);
https://doi.org/10.1016/S1003-6326(10)60502-X
111. L. Yao, H. Hao, S.-H. Ji, C.-F. Fang, and X.-G. Zhang, Effects of Ultrasonic Vibration on Solidification Structure and Properties of Mg–8Li–3Al Alloy, *Trans. Nonferrous Met. Soc. China*, **21**: 1241 (2011);
https://doi.org/10.1016/S1003-6326(11)60848-0

112. M.H. Khan, A. Das, T.I. Khan, Z. Li, and H.R. Kotadia, Microstructural Modification in an Al–Mg–Si (6082) Alloy with High Fe Content Using Inoculation and/or High-Intensity Ultrasonication, *J. Alloys Compd.*, **1012**: 178500 (2025); https://doi.org/10.1016/j.jallcom.2025.178500
113. M. Li, T. Tamura, N. Omura, Y. Murakami, and S. Tada, Grain Refinement of AZCa912 Alloys Solidified by an Optimized Electromagnetic Stirring Technique, *J. Mater. Process. Technol.*, **235**: 114 (2016); https://doi.org/10.1016/j.jmatprotec.2016.04.024
114. D.A. Lesyk, B.M. Mordyuk, W. Alnusirat, S. Martinez, V.V. Dzhemelinskyi, O.O. Honcharuk, P.V. Kondrashev, Yu.V. Kliuchnykov, and A. Lamikiz, Ultrasonic Surface Finishing of AISI 1045 Steel Hardened by Laser Heat Treatment with Fibre Laser and Scanning Optics: Layered-Structure-Induced Hardening and Enhanced Surface Morphology, *Prog. Phys. Met.*, **25**, No. 4: 822 (2024); https://doi.org/10.15407/ufm.25.04.822
115. F. Jiang, K.-Q. Qiu, H.-D. Wang, Q.-C. Xiang, Y.-R. Zhang, and Y.-D. Qu, Effects of Bi Modification and Ultrasonic Treatment on Microstructure Evolution and Mechanical Properties of AlMg5Si2Mn Alloy, *J. Alloys Compd.*, **901**: 163486 (2022); https://doi.org/10.1016/j.jallcom.2021.163486
116. A. Isagulov, R. Sultangaziyev, V. Kulikov, A. Akberdin, and A. Kim, Diagram of Equilibrium Phase Composition of Fe–C–Si–B System, *Metalurgija*, **55**, No. 3: 305 (2016).
117. D. Aubakirov, A. Issagulov, S. Kvon, V. Kulikov, Y. Chsherbakova, and S. Arinova, Modifying Effect of a New Boron–Barium Ferroalloy on the Wear Resistance of Low-Chromium Cast Iron, *Metals*, **12**: 1153 (2022); https://doi.org/10.3390/met12071153
118. P.V. Kovalev, S.D. Popova, A.Z. Issagulov, V.Y. Kulikov, and S.S. Kvon, Investigation of the Effect of High Strength Strips Steel Modification with Rare-Earth Metal (REM), *Metalurgija*, **56**, Nos. 3–4: 393 (2017).
119. X. Liu, Z. Guo, J. Xue, and C. Zhang, Ultrason. *Sonochem.*, **52**: 33 (2019); https://doi.org/10.1016/j.ultsonch.2018.09.009
120. L. Zhang, X.-Q. Li, S. Ge, G. Huang, R.-P. Jiang, J.-P. Xie, and S.-K. Guan, Trans. Nonferrous Met. *Soc. China*, **35**, No. 5: 1381 (2025); https://doi.org/10.1016/s1003-6326(24)66755-5
121. I.V. Gomes, M. Pacheco, M. Nienaber, S.C. Neves, D. Mei, A. Barros, R.L. Reis, J.L. Alves, and H. Puga, *J. Magnes. Alloys*, **11**, No. 8: 2901 (2023); https://doi.org/10.1016/j.jma.2023.07.013

Received / Final version
03.07.2025 / 24.01.2026

А.З. Ісагулов, В.Ю. Куліков, С.В. Квон, С.К. Арінова, А.А. Туганбаєва
Карагандинський технічний університет імені Абилкаса Сагінова,
просп. Нурсултана Назарбаєва, 56; 100003 Караганда, Казахстан

СУЧАСНІ ТЕНДЕНЦІЇ У ВИРОБНИЦТВІ ВИЛИВКІВ
ІЗ ЧОРНИХ І КОЛЬОРОВИХ СПЛАВІВ З ВИКОРИСТАННЯМ
ЗОВНІШНІХІ ВНУТРІШНІХ ВПЛИВІВ

Узагальнено сучасні дані стосовно методів рафінування та гомогенізації структур металевих сплавів із застосуванням внутрішніх хімічних модифікаторів і зовнішніх фізичних полів. Проаналізовано механізми, за допомогою яких наночастинки, рідкісноземельні елементи й інокулянти сприяють гетерогенному зародженню кристалів і керують динамікою кристалізації. Оцінено вплив механічних коливань, ультразвуку й електромагнетних полів на морфологію зерна, фазову однорідність і поведінку включень. Особливу увагу приділено синергічній дії зазначених методів для формування армованих або композитоподібних мікроструктур з поліпшеними механічними та функціональними характеристиками. Критично оцінено наявні дані та запропоновано концептуальну основу для подальших досліджень стратегій оброблень розплаву, спрямованих на створення матеріалів із заданими властивостями для перспективних застосувань.

Ключові слова: внутрішнє модифікування, зовнішні поля, механізми кристалізації, гетерогенне зародження, синергічне оброблення, мікроструктура сплаву.